

**Quantum Evolutionary Algorithm Based High Performance Control of  
Induction Motor Drive Using ANN Flux Estimator**

by

**Md. Habibullah**



A thesis submitted in partial fulfillment of the requirements for the degree of  
Master of Science in the Department of Electrical and Electronic Engineering



Khulna University of Engineering & Technology

Khulna 9203, Bangladesh

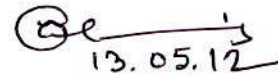
**May 2012**

## Declaration

This is to certify that the thesis work entitled "*Quantum Evolutionary Algorithm Based High Performance Control of Induction Motor Drive Using ANN Flux Estimator*" has been carried out by *Md. Habibullah* in the Department of *Electrical and Electronic Engineering*, Khulna University of Engineering & Technology, Khulna, Bangladesh. The above thesis work or any part of this work has not been submitted anywhere for the award of any degree or diploma.

  
13.05.12

Signature of Supervisor  
(Prof. Dr. Md. Abdur Rafiq)

  
13.05.12

Signature of Candidate  
(Md. Habibullah)

## Approval


This is to certify that the thesis work submitted by *Md. Habibullah* entitled " *Quantum Evolutionary Algorithm Based High Performance Control of Induction Motor Drive Using ANN Flux Estimator* " has been approved by the board of examiners for the partial fulfillment of the requirements for the degree of *Master of Science* in the *Department of Electrical and Electronic Engineering*, Khulna University of Engineering & Technology, Khulna, Bangladesh in May 2012.

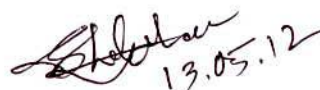
### BOARD OF EXAMINERS


1. Professor Dr. Md. Abdur Rafiq  
Dept. of Electrical and Electronic Engineering  
Khulna University of Engineering & Technology  
Khulna-9203, Bangladesh.
2. Professor Dr. Md. Abdur Rafiq  
Head, Dept. of Electrical and Electronic Engineering  
Khulna University of Engineering & Technology  
Khulna-9203, Bangladesh.
3. Professor Dr. Md. Rafiqul Islam  
Dept. of Electrical and Electronic Engineering  
Khulna University of Engineering & Technology  
Khulna-9203, Bangladesh.
4. Dr. Md. Shahjahan  
Associate Professor  
Dept. of Electrical and Electronic Engineering  
Khulna University of Engineering & Technology  
Khulna-9203, Bangladesh.
5. Professor Dr. Bashudeb Chandra Ghosh  
Dept. of Electrical and Electronic Engineering  
American International University-Bangladesh  
Dhaka-1213, Bangladesh.

  
13.05.12  
Chairman  
(Supervisor)

  
13.05.12  
Member

  
Member

  
13.05.12  
Member

  
13.05.12  
Member  
(External)

Dedicated  
To  
My Beloved Parents  
&  
Respected Teachers

## Acknowledgements

I wish to express my most sincere gratitude to my supervisor, Professor Dr. Md. Abdur Rafiq, for the substantial guidance and support given in scientific writing, and for the valuable opinions expressed during the year. Special thanks go to Prof. Dr. B. C. Ghosh for providing preliminary directions including initial literature on the subject, and for pointing out valuable comments.

I want to thank Dr. Md. Shahjahan for sharing his idea about chaos and proofreading of part of Chapter 4 and many educational discussions in it we had. I would also like to thank Mr. Md. Amjad Hossain for sharing his idea about Quantum Evolutionary Algorithm.

I would like to thank Dr. Md. Rafiqul Islam for his constant inspiration towards this work. I would also like to thank to the Head of the Department of Electrical and Electronic Engineering for providing me all possible facilities without which I could not think of the completion of research work.

Finally, I would like to thank my family for the love and support they have been giving during the years of my studies.

Khulna, 13.05.2012

Md. Habibullah



## Abstract

In this study, Quantum Evolutionary Algorithm (QEA) based high performance control of induction motor is proposed, whose rotor flux is estimated by chaotic learning based Artificial Neural Network (ANN). The control principle is based on Direct Torque Control (DTC) with Space Vector Modulation (SVM) technique. The SVM reduces the torque and flux ripples and improves steady state performance. Fast dynamic speed response is obtained through maintaining the rotor flux constant as in the case of field orientation control. Main flux saturation effect is also considered throughout the study for more realistic representation in the analysis. QEA based proportional-integral (PI) controller tuning is used for getting optimized gain coefficients of PI controller which also help us to get fast speed response induction motor drive. The performance of the drive system with QEA based PI controller is compared with Conventional Genetic Algorithm (CGA) based PI controller. There is no speed fluctuation in the speed response of QEA based induction motor drive under steady state condition whereas a little bit speed fluctuation is present in the CGA based induction motor drive.

In this work, chaotic learning based Artificial Neural Networks (ANNs) such as Backpropagation (BP), Real Time Recurrent Learning (RTRL), and Correlated Real Time Recurrent Learning (CRTRL) are proposed for improved rotor flux estimation of induction motor drive which makes the control system position sensorless. Chaotic variations of learning rate are included with the learning rate of BP, RTRL, and CRTRL algorithms based ANNs which generates a chaotic time series and a rescaled version of the series is used as Learning Rate (LR) during the training process. We have shown the improvement of BP and CRTRL algorithm based ANNs in rotor flux estimation of induction motor drive due to the use of chaotic variations in learning rate.

A high performance simple speed estimator is also presented in this work. It is confirmed that the proposed speed estimator is capable to estimate the speed accurately even at very low speed. Effectiveness of the proposed controller is tested by simulation for different set speed. This simple speed estimator for the induction motor drive makes the controller cost effective and sensorless. Robustness of the control system is tested by using the parameter perturbation and applying sudden load torque disturbance within very short time interval. The control system is also computationally efficient and tested by introducing 10% instrumental error to reference voltage vectors.

# CONTENTS

	PAGE	
Title Page	i	
Declaration	ii	
Certificate of Research	iii	
Acknowledgement	v	
Abstract	vi	
Contents	vii	
List of Tables	ix	
List of Figures	x	
List of Abbreviations	xii	
Nomenclature	xiii	
<b>CHAPTER I</b>	<b>Introduction</b>	
1.1	Introduction	1
1.2	Literature Review	2
1.3	Motivation and Scope of the Present Study	4
1.4	Thesis Overview	5
<b>CHAPTER II</b>	<b>Mathematical Models of Induction Motor Drives</b>	
2.1	Introduction	7
2.2	Induction Motor Model	7
2.2.1	Stationary Two-Axis Model	7
2.2.2	Synchronously Rotating Two-Axis Model	9
2.3	Phase Relationship	11
2.4	Induction Motor Model in Terms of Stator Current and Rotor Flux	12
2.5	Induction Motor Model under Field Orientation Principle	13
2.6	Analysis of Magnetization Characteristics	14
2.7	Conclusion	16
<b>CHAPTER III</b>	<b>QEA and Fast Speed Response IM Drive</b>	
3.1	Introduction	17
3.2	Conventional Genetic Algorithm (CGA)	17
3.3	Quantum Evolutionary Algorithm (QEA)	19
3.3.1	Representation of QEA	19
3.3.2	Procedure of QEA	20
3.4	Comparative Analysis between QEA and CGA Based IM Drive	22
3.4.1	Transient and Steady State Performance	22
3.4.2	Fast Speed Response IM Drive	23
3.5	Conclusion	24
<b>CHAPTER IV</b>	<b>Chaotic Learning Based ANN</b>	
4.1	Introduction	25
4.2	Chaos Variables	25
4.3	Chaotic Learning Based Back-Propagation Algorithm	26
4.4	RTRL and CRTRL Algorithm for ANN	28
4.5	Simulation Results	32
4.6	Conclusion	34

<b>CHAPTER V</b>	<b>Proposed Control Methodology and Simulation Study</b>	
	5.1 Introduction	36
	5.2 Space Vector Definition	36
	5.3 Space Vector Modulation	38
	5.3.1 Proposed Control Scheme	38
	5.3.2 Simulation Model	39
	5.3.3 The Speed Estimator	41
	5.4 Simulation Study	41
	5.4.1 Effects of Magnetic Saturation on Induction Motor Drive	41
	5.4.2 Starting Performance of the Induction Motor Drive	43
	5.4.3 Performance under Different Operating Conditions	44
	5.4.4 Performance under Parameter Deviation Conditions	47
	5.4.5 Robustness against Computational Error	48
	5.4.6 Speed Estimation and Dynamic Behavior	48
	5.5 Conclusion	50
<b>CHAPTER VI</b>	<b>Conclusions</b>	
	6.1 Conclusion	52
	6.2 Proposal for Further Research	53
	<b>References</b>	54
	<b>Appendix</b>	58
	List of Publications on This Thesis	59



## LIST OF TABLES

Table No	Description	Page
3.1	Mean Square Error Comparison	31
Table App. 1	Induction Motor Parameters and Nameplate Data / Rating	58



## LIST OF FIGURES

Figure No.	Description	Page
2.1	Physical Coil system of the stator and the rotor of a 3-phase induction motor	8
2.2	Mutually perpendicular fictitious coils of the 3-phase equivalent of induction motor	9
2.3	Relation between various co-ordinate systems and principle of field orientation	11
2.4	Physical 3-phase variables and their equivalent fictitious two-axis phasors	11
2.5	Magnetization characteristics (a) true saturation characteristic and (b) magnetizing inductance	15
3.1	Evolution Procedure of CGA.	18
3.2	Overall structure of QEA	21
3.3	Updating of two gains (a) $k_p$ and (b) $k_i$ using CGA and QEA	21-22
3.4	Speed response of QEA and CGA based PI controller	22
3.5	Zoomed Speed response of QEA and CGA based PI controller at (a) Transient condition for the time 0 to 1sec. (b) Steady state condition for the time 1 sec. to 3 sec. of Fig. 3.4	23
3.6	Speed response of IM drive using conventional PI controller and QEA based PI controller with different set speed	23
4.1	The logistic mapping	25
4.2	Fully connected real time recurrent network	28
4.3	Stationary $\alpha$ - and $\beta$ - axes rotor flux synthesis by CRTRL algorithm	30
4.4	(a) Mean square error comparisons between Back-propagation, RTRL and CRTRL algorithms using chaotic learning based ANN (b) Small scale representation of MSE for chaotic learning based CRTRL.	31
4.5	Actual and estimated $\alpha$ -axis rotor flux synthesis using backpropagation algorithm (a) transient and (b) steady state.	32

4.6	Actual and estimated $\beta$ -axis rotor flux synthesis using BP algorithm (a) transient and, (b) steady state	33
4.7	Actual and estimated $\alpha$ -axis rotor flux synthesis using CRTRL algorithm (a) transient and, (b) steady state	33-34
4.8	Actual and estimated $\beta$ -axis rotor flux synthesis using CRTRL algorithm (a) transient and, (b) steady state	34
5.1	Space vector modulation signal flow diagram	36
5.2	Switching-state vectors, shown in the first $60^\circ$ sector, (b) All voltage vectors in space	37
5.3	Proposed control scheme	40
5.4	Effects of considering magnetic saturation (a) speed response, (b) three phase stator current, and (c) developed electromagnetic torque under transient and steady-state condition.	42
5.5	Simulated (a) speed response, (b) developed electromagnetic torque, and (c) rotor flux under transient and steady-state condition.	43-44
5.6(a)	Performances of the induction motor drive under speed reversal condition at transient and steady state condition.	44-45
5.6(b)	Performances of the induction motor drive with step change in speed at transient and steady state condition.	45
5.6(c)	Performances of the induction motor drive with ramp change in speed at transient and steady state condition.	45-46
5.6(d)	Performances of the induction motor drive with step change of load at transient and steady state condition.	49
5.7	Performances of the induction motor drive for change in stator and rotor resistances with (a) $R_s = 2R_s^*$ , and (b) $R_r = 2R_r^*$ at $t=1$ second.	47-48
5.8	Performances of the induction motor drive under computational errors present in the physical system.	48
5.9	Simulated (a) actual and estimated speed responses (b) estimated electromagnetic torque, and (c) estimated rotor flux under transient and steady-state conditions.	49
5.10	Simulated (a) actual and estimated speed responses (b) estimated electromagnetic torque, and (c) estimated rotor flux under transient and steady state conditions.	50

## LIST OF ABBREVIATIONS

IM	Induction Motor
DTC	Direct Torque Control
PWM	Pulse Width Modulation
SVM	Space Vector Modulation
HPC	High Performance Control
AI	Artificial Intelligence
FO	Field Orientation
FOC	Field Orientation Control
ANN	Artificial Neural Network
BP	Backpropagation
GA	Genetic Algorithm
PSO	Particle Swarm Optimization
DE	Differential Evolutionary
EA	Evolutionary Algorithm
QEA	Quantum Evolutionary Algorithm
CGA	Conventional Genetic Algorithm
RTRL	Real Time Recurrent Learning
CRTRL	Correlated Real Time Recurrent Learning
LR	Learning Rate
RNN	Recurrent Neural Network
MSE	Mean Square Error
MMF	Magnetomotive Force
EMF	Electromotive Force
PI	Proportional-Integral
TVM	Time Variant Mutation
MLP	Multilayer Perceptron
6S3P	Six Switch Three Phase

## NOMENCLATURE

$G$	gain function
$L$	self-inductance
$R$	internal resistance
$L_m$	mutual inductance
$\omega_r$	angular velocity
$\alpha, \beta$	orthogonal axes of stationary reference frame
$d - q$	synchronously rotating reference frame
$x - y$	rotor fixed reference frame
$P_p$	number of pole pairs
$v_{\alpha s}, v_{\beta s}$	$\alpha$ -and $\beta$ -axis stator voltage components
$v_{ds}, v_{qs}$	d-and q-axis stator voltage components
$i_{\alpha s}, i_{\beta s}$	$\alpha$ -and $\beta$ -axis stator current components
$i_{\alpha r}, i_{\beta r}$	$\alpha$ -and $\beta$ -axis rotor current components
$i_{ds}, i_{qs}$	d-and q-axis stator current components
$J$	moment of inertia
$B$	rotational damping coefficient
$\omega_m$	angular speed of the motor
$T_L$	load torque
$\omega_e$	synchronous reference speed
$\omega_r$	rotor angular speeds
$\omega_{sl}$	angular slip speed
$R_s, R_r$	stator and rotor resistances
$\bar{\psi}_s$	stator flux linkage vector
$\bar{\psi}_s^s = [\psi_{ds}, \psi_{qs}]^T$	stator flux linkage vector
$\bar{\psi}_r^s = [\psi_{dr}, \psi_{qr}]^T$	rotor flux linkage vector
$\bar{\psi}_r$	rotor flux linkage vector

$a_s$	actual stator a phase axis
$a_r$	actual rotor a phase axis
$p$	derivative of time
$\sigma$	leakage coefficient
$L_m$	Mutual inductance
$\bar{i}_s$	primary or stator current vector
$\bar{v}_s$	primary or stator voltage vector
$\theta_s$	stator flux angle
$\theta_r$	rotor flux angle
$\hat{\theta}_s$	estimated stator flux angle
$\hat{\theta}_r$	estimated rotor flux angle
$\alpha_s$	stator current angle
$\tau$	torque error
$\Phi$	flux error
$T_e$	estimated electromotive torque
$\psi_s$	estimated stator flux linkage
$\psi_r$	estimated rotor flux
$i_{Sa}$	stator a-phase current
$i_{Sb}$	stator b-phase current
$v_a$	stator a-phase voltage
$v_b$	stator b-phase voltage
$v_c$	stator c-phase voltage
$\psi_s^*$	stator command flux
$\omega_m^*$	motor command speed
$T_e^*$	motor command torque
$\bar{u}^*$	reference voltage vector
$\bar{u}^*(T_s)$	sampled value reference voltage vector
$\bar{u}^*(t)$	reference vector

$T_s$	sampling time
$f_s$	sampling frequency
$\bar{u}_a$	switching state vector, a
$\bar{u}_b$	switching state vector, b
$t_a$	duration of the switching state vectors $u_a$
$t_b$	duration of the switching state vectors $u_a$
$t_0$	duration of the switching state vectors $u_0$
$i_{ds}^*$	the d-axis reference current
$i_{qs}^*$	the q-axis reference current
$v_{ds}^*$	the d-axis reference voltage
$v_{qs}^*$	the q-axis reference voltage
$\alpha(0)$	probability of 0 state
$\beta(1)$	probability of 1 state
$F$	fitness function
$Q(t)$	population of qubit chromosomes
$P(t)$	set of binary solution
$U(t)$	quantum gates
$B(t)$	better solution
$\varsigma$	speed error
$k_p$	proportional gain coefficient
$k_i$	integral gain coefficient
$b_k$	bias of the neuron k
$w_{km}$	synaptic weight of the neuron k to m
$u_k$	linear combiner output due to the input signals
$\varphi(\cdot)$	activation function
$y_k$	output signal of the neuron k
$x(n)$	signal vector at the time step $n$
$d_k(n)$	target output at the time step $n$
$e_k(n)$	error signal at the time step $n$
$\zeta(n)$	cost function at the time step $n$
$\eta$	rate of learning

$\gamma$	chaotic learning rate
$Z^{-1}$	unit-delay operator
$a$	slope parameter of the sigmoid function
$\varepsilon ( n )$	instantaneous value of total error energy
$\varepsilon_{av}$	average squared error energy
$\delta_j(n)$	local gradient at the time step $n$
$\varphi_j'(v_j(n))$	derivative of the associated activation function
$z(k)$	the $(q+m+1)$ -by-1 vector
$\Lambda_j(k)$	partial derivative matrix of the state vector $x(n)$ with respect to the weight vector $w_j$
$Z_i(k)$	$q$ -by- $(q + m + 1)$ matrix whose rows are all zero
$\varphi(k)$	$q$ -by- $q$ diagonal matrix whose $k$ th diagonal element is the partial derivative of the activation function with respect to its argument
$\tilde{y}(k)$	desired output vector
$\zeta$	objective function





## CHAPTER I

### Introduction

#### 1.1 Introduction

AC motors, especially induction motors are suitable for industrial drives, because of their simple and robust structure, high torque to weight ratio, higher reliability and ability to operate in hazardous environments. However, the control of induction motor is a challenging task as the rotor quantities are not accessible which are responsible for torque production. DC machines are decoupled in terms of flux and torque. Hence control is easy. If it is possible in case of induction motor to control the amplitude and space angle (between rotating stator and rotor fields), in other words to supply power from a controlled source so that the flux producing and torque producing components of stator current can be controlled independently, the motor dynamics can be compared to that of DC motor with fast transient response. Presently, introduction of micro-controllers, high switching frequency semiconductor devices, and VLSI technology has led to cost effective sophisticated control strategies.

A new area of ac motor drive has been highly developed by power electronics technology. In particular, squirrel cage induction motor drive "under the vector control of induction motor drive" is considered as one of the best ac variables controlled drives when quick response is required. The stator current is splitted into two orthogonal components, one in the direction of flux linkage, representing magnetizing current or flux component of current and other perpendicular to the flux linkage, representing the torque component of current. By varying both components independently, the induction motor can be treated as a separately excited DC motor. This concept was invented in the beginning of 1970s. The implementation of vector control requires information regarding the magnitude and position of the flux vector. Depending upon the method of acquisition of flux information, the vector control or field oriented control method can be termed as: direct or indirect. In the direct method the position of the flux is strictly measured with the help of sensors, or estimated from the machine terminal variables such as speed and stator current/voltage signals. The measured or estimated flux is used in the feedback loop, thus the machine parameters have minimal effect on the overall drive performance. But the measurement of flux using flux sensors necessitates special manufacturing process or modifications in the existing machines. In addition, the direct field orientation method has its inherent problem at low speed where the voltage drops due to resistances are dominant, and pure integration is difficult to achieve.

Recently, advanced control strategies for Pulse Width Modulation (PWM) inverter fed induction motor drive has been presented. Particularly, the vector control, which guarantees high dynamic and static performances like DC motor drives, has become very popular and has been developed and improved. Recent developments in the theory of vector control, fast digital processor and power devices provide the possibility of achieving high performance induction motor drive control.

Space Vector Modulation (SVM) technique is widely used in control of induction motor drive. This technique reduces the torque and flux ripple in induction motor drive and high performance is achieved. It contains space vectors to be applied according to the region

where the output voltage vector is located. It has two excellent features such as maximum output voltage is greater and the number of switching is less at the same carrier frequency.

High performance drive of an induction motor requires the rotor position information to control the motor which is generally detected by mechanical position sensors such as an encoder or a resolver. The additional components such as resolver and position sensors not only increase the cost but also affect reliability of the system. Flux estimation can be applied to find the rotor position and is considered as an important task in implementing high performance motor drives.

Unfortunately observer or flux estimator has some inherent disadvantages, such as the influence of noise, the computational burden. This has led to a renewed interest to the field of flux estimation. Recently, AI (artificial intelligent) techniques such as expert system, fuzzy logic, and artificial neural networks (ANN) are showing much promise for intelligent adaptive control and estimation of parameters and variables of motor drives. The machine terminal voltages and currents can be sensed and processed to calculate speed, position, flux, torque, power and other feedback signals with the help of a microprocessor. The inaccuracy of estimated signals due to machine parameter variation always remains a problem. Accurate identification of machine parameters to compensate the estimation error is a challenging task. In addition, direct integration of machine voltages near zero speed to calculate the flux is another problem because of offset problem of the integrator. The flux of a machine can be conveniently estimated from the stator voltage model at higher speed range and rotor current model at low speed range. The stator flux can be estimated using ANNs for better accuracy.

Recent trend in the field of induction motor control mainly try to incorporate the features of ANNs, Fuzzy logic, Genetic and Evolutionary Algorithms. These components of Artificial Intelligence (AI) provides accurate, robust and show insensitivity to parameter deviations. These computational methods are generally applied to estimate the rotor flux of induction motor drive and to tune or upgrade controller constants.

## **1.2 Literature Review**

At present induction motors are widely used for variable speed energy converting devices in industrial and domestic appliances. They are simple, rugged, inexpensive and available at all power ratings. Progress in the field of power electronics and microelectronics enables the application of induction motors for high performance drives, where traditionally only DC motors were applied [1]. Speed and torque control mechanisms are very much essential in recent electrical motor drives [2-3].

High Performance Control (HPC) of induction motors is an interesting area for research and has wide applications in lathe machines, robotics etc. The main objective of high performance controller is to obtain fast dynamic response of the drive system. It is so designed that it becomes less sensitive to motor and controller parameter perturbations and require minimum hardware for its practical implementation.

The field-oriented control (FOC) technique is widely used in high performance motion control of induction motors. Because of torque/flux decoupling, FOC achieved good dynamic response and accurate motion control as separately excited dc motors. Two types of field orientation control schemes are used for induction motor control; first one is direct and the other is indirect control methods. In the indirect control method, the major problem is the rotor time constant, which is sensitive to both the temperature and flux level variations. When the estimation of this parameter is incorrect, the slip frequency is also

incorrect and flux angle is no longer appropriate for field-orientation [4]. Direct field-orientation control is sensitive to stator resistance and total leakage inductance. In direct field-orientation, if a flux regulator is employed, the parameter sensitivity is less than the indirect field-orientation control. In an induction motor under field-orientation control, the flux can be adjusted to meet control requirement than that of permanent magnet motor field-orientation [5].

The control objective requires the rotor position and/or speed of the motor to follow a preselected time tagged trajectory, regardless of unknown load variation and other parameter uncertainties. The additional components such as resolver and position sensors not only increase the cost but also affect reliability of system. Flux estimation can be applied to find the rotor position and is considered as an important task in implementing high performance motor drives.

The Engineering community has shown a significant interest in optimization for many years [6-8]; in particular, there has been a focus on global optimization of numerical, real-valued problems for which exact and analytical methods do not function suitably. During the last few decades, a number of general-purpose optimization algorithms have been proposed for finding optimal solutions, some of which are; Evolution Strategies [9], Evolutionary programming [10], Genetic Algorithm (GA) [11], Particle Swarm Optimization (PSO) [12] and Differential Evolution (DE) [13]. These algorithms are also known as Evolutionary Algorithms (EAs) or Nature Inspired Algorithms because they follow simple rules of nature. These algorithms have also become popular because of their advantages over the traditional optimization techniques. The optimization performance of all the algorithms mentioned above degrades with a small population and cannot optimize the solution within a very short time.

Quantum Evolutionary Algorithm (QEA) is a novel probability optimization algorithm based on the concept and principles of quantum computing [14]. Compared with Conventional Genetic Algorithm (CGA), QEA has a better characteristic of diversity in the population and can keep the balance of exploration and exploitation more easily- even with a small population. So QEA has become a research hotspot in recent years.

The application of ANN attracts the attention of many scientists from all over the world [15]. The reason for this trend is the many advantages which the architectures of NN have over traditional algorithmic methods. Among the advantages of ANN, the ease of training and generalization, simple architecture, possibility of approximating nonlinear functions, insensitivity to the distortion of the network, and inexact input data are worth mentioning. The main problem of ANNs such as BP and RTRL algorithms is that the optimal procedure is easily trapped into local minimum value and the speed of convergence is very slow. To avoid this problem, non-uniform periodicity property of chaos is used in [16-17] and starts its improvement from the learning rate. In [16], the authors show that the improved algorithm is not only efficient in internet traffic prediction with higher precision and faster speed of convergence, but also somewhat escapes the network from the problem of local minima. In [17], the authors show that, if the chaotic variation learning rate (LR) is included during training, the weight update may be accelerated in the local minimum zone.

The neural networks have become well established in induction motor drive for different tasks especially for flux estimation. Since the 1990s, several investigations into the applications of neural networks in the field of electrical machines and power electronics have appeared [18]. A new form of implementation of filter is proposed for stator flux

vector synthesis that uses a combination of recurrent neural network trained by Kalman filter and a polynomial neural network in [19]. Correlated real time recurrent learning (CTRL) neural networks has been introduced in [20] that uses  $\alpha$ - and  $\beta$ -axis flux components coupling for the flux estimation rather decoupling them.

Incorporation of chaos in induction motor is recently a hot topic in research area. Researchers consider chaotic properties for different aspects to induction motor in [21-23]. A new chaotic pulse width modulation (PWM) scheme is proposed and implemented for AC motors, which functions to suppress significantly the harmonic peaks and hence the acoustic noise in [21-22]. In [23], the authors propose a new application of a chaos particle swarm optimization (PSO) algorithm for loss model-based energy efficient control of an induction machine (IM) using an optimal rotor flux reference. The flux observers based on recurrent neural network (RNN) methods are implemented in [24] in which mean square error (MSE) values of the rotor flux estimation are between 0.000087 and 0.000264. But yet now, no literature is available to the authors for chaotic learning based ANN for flux estimation of induction motor drive.

To exploit the benefits of sensorless control, the speed estimation methods must achieve robustness against model and parameter uncertainties. Parameters of particular concern in the sensorless control literature are frequency-dependent  $R_r$  and temperature-dependent  $R_s$  and the load torque, all of which are very effective on the accurate estimation of flux and speed. To address the parameter sensitivity problem in induction motor speed sensorless control, a variety of approaches have been proposed [25-27]. But low speed estimation is a problem there. A Lyapunov-function based flux and speed observer was developed [28] which can estimate  $R_s$  but not  $R_r$ . Duran et al. [29] performed a thermal-state estimation to compensate for the parameter and hence speed deviations due to heating. All researchers mentioned above proposed sensorless controller for induction motor drive and they didn't consider the saturation effects in induction motor drive. But it is well known that consideration of saturation effect improves the dynamic characteristics of induction motor drive.

### **1.3 Motivation and Scope of the Present Study**

High performance induction motor drives are very much popular at the present day industries. There are various control laws to implement these high performance drives. The drive technologies are now in matured state. However, a good number of researchers have been working in this field to improve the control methodologies. The control laws related to high performance drives are very interesting and the author felt encouraged to work in this area. Induction motors are still the most used industrial motor and need to be studied for high performance applications.

The three main features of high performance control are the field orientation control, direct torque control and the space vector modulated inverter feeding the motor. Normally, three techniques are used independently in high performance control of induction motors. Each has great advantages along with some disadvantages. These advantages may be combined to have a very prospective high performance control. There is huge scope to work in this field.

Many control laws are available to control the induction motor. The schemes are Direct Torque Control (DTC), Space Vector Modulation (SVM), voltage and current based angle control, load angle estimated based control, Field-Oriented (FO) based Control, etc. The transient response of DTC controller is better but it creates some ripple in the steady state,

whereas SVM is suitable for not only minimize the ripple but also number of switching states. This thesis implements SVM technology with applying DTC principle for fast speed response and applying field orientation technique to process the error through PI controller of the induction motor drive. For implementing the SVM technique, the exact stator flux and the electromagnetic torque information of an induction motor is needed. To estimate the flux and torque, some algorithm is used for eliminating the sensors. Different types of observers, artificial intelligent based estimator may be used. These observers have some limitations to estimate the rotor flux under miss-match parameter condition of the controller. Some adaptation technique is used to overcome the limitations. This adaptation arises some complexity in controller. It is possible to design a simple controller using artificial neural network (ANN). ANN has different computational method to obtain gradient for estimating purpose. It may be trained on-line or off-line. For learning this various computing techniques are used like back-propagation, real time recurrent learning (RTRL) etc. For the existence of hidden layers back-propagation arise computational burden. RTRL has no hidden layer and it reduce the computation burden. Again it estimates the rotor flux accurately even any parameter miss-match condition and filter any disturbance noise.

In this thesis, PI controller based voltage vector controlled SVM controller is proposed. The gain coefficients of PI controller are optimized by quantum evolutionary algorithm. A new stable method of estimating rotor flux and torque has been proposed. The proposed scheme is chaotic learning based real time recurrent learning (RTRL) algorithm to estimate rotor flux. RTRL networks are basically dynamic systems where the states evolve according to certain nonlinear state equation. Several training methods have been developed. These are basically different in computation to obtain gradient. Some of these methods compute the gradient very efficiently. However, the main shortcoming of these methods is the excessive number of iteration needed to reach the minima. RTRL has no hidden neuron, less computational burden and can be easily implemented practically. The goal of this thesis work is to overcome the limitation and develop a new recurrent network algorithm to estimate the induction motor rotor flux accurately even under parameter mismatch condition between motor and controller.

This thesis describes a high performance induction motor drive combining the principle of DTC, FO and SVM for fast transient response and also operates in vector control mode. Improved chaotic learning based correlated RTRL based flux and torque estimators are used. The saturation characteristics in the magnetic circuit of induction motor drive also provides better dynamic performance. Hence main flux saturation effect is considered as a variable magnetizing inductance throughout the work. Simulation and experimental results justified the excellent operating characteristics of the drive as a high performance induction motor drive.

#### **1.4 Thesis Overview**

The present thesis is organized in the following way.

Chapter-I begins with a preliminary discussion on drive systems, inverters, field oriented control pertaining to induction motor and related controller law. This is followed by an overview of a few selected contributions to indicate, in brief, the various studies that have been made over the past three decades in the area of vector controlled induction motor. It also includes the scope of the present study. The chapter concludes the contents of the study of other chapters in brief.

Chapter-II commences with the two-axis model of the induction machine in both stationary and synchronous reference frames with their phase relationship. The mathematical models are written in different formats to represent the induction motor under different operating conditions. The magnetic nonlinearity has been modeled by polynomial fit curve and polynomial fitted mutual inductance is included to consider saturation effects are also included in this chapter.

Chapter-III presents quantum evolutionary algorithm (QEA) and conventional genetic algorithm (CGA), discussing their performance in the control system for induction motor drive. In the view of the different conditions, QEA based proportional-integral (PI) controller is chosen and used for the remain of the research work.

Chapter-IV discusses on flux estimators for induction motors. Preliminary idea of ANN and its learning techniques especially back propagation, RTRL and proposed chaotic learning based CRTRL algorithms for the ANN are discussed in this chapter. It also contains the performances of all above the flux estimators as a comparison and chaotic learning based CRTRL is used for the remain of the research work.

Chapter-V covers the formulation of the proposed control system. The performances of the control method with different operating conditions including the abnormalities are included. Simulation model of the machine is deduced and results of simulation under different operating conditions are shown. An endeavor is also made in this chapter to make the control system speed sensorless and effectiveness of the controller is also tested for different conditions.

Finally chapter-VI includes the overall conclusions of this research work and highlights the direction of further research.

## CHAPTER II

### Mathematical Models of Induction Motor Drives

#### 2.1 Introduction

A poly-phase induction motor has a complex structure comprising of mutually coupled magnetic and electric circuits. When the stator coils are excited by balanced electrical source, flux produced in the stator core sweeps past to the rotor core. The rotor coils are shorted together at both ends with the rotor bars in a squirrel cage induction motor. The mutual flux system is common to coils both in stator and rotor and is responsible for the effective operation of the motor. The leakage flux is responsible for causing voltage drop in the coils. Due to mutual coupling between stator and rotor coils, rotor receives power by induction. There are three systems of flux that may be considered in an induction motor, viz, the stator flux, the air gap flux and the rotor flux. In a dc motor, torque is viewed as the product of field flux and armature mmf, which are mutually perpendicular to each other. Similarly, in an induction motor it can be assumed that the flux of rotor and perpendicular mmf in the stator or vice versa generates the electromagnetic torque. Other viewpoint assumes power in the rotor resistance as a measure of torque expressed in synchronous watts.

To study the performance of different control systems and drives, the motor requires to be represented by a set of differential equations in time domain. Complexity arises due to variable coupling between the physical coils of the stator and the rotor. The complexity is further enhanced due to the effect of back emf in the rotor circuit. So it is not wise to model an induction motor using the physical coils.

Based on operating conditions, there are a number of mathematical models for induction motors. Mutually perpendicular stationary and synchronously rotating fictitious coils are considered to study the transient and dynamic conditions of induction motor drives.

#### 2.2 Induction Motor Model

In an induction motor the stampings form the core which is slotted to receive the three phase windings of the stator. The windings are fed from a three phase supply. The rotor also consists of core for carrying three phase winding bars. Mathematically, a winding can be modeled as self-inductance  $L$  and some internal resistance  $R$ . Suffices  $s$  and  $r$  are introduced to indicate stator and rotor circuits respectively. The transfer of energy from stator to rotor of an induction motor takes place entirely inductively with the help of a flux mutually linking the two. That is why mutual inductance  $L_m$  exists between the two.

It is well documented in the literature that an induction motor can adequately be modeled using a two-axis reference frame. Under the usual assumptions of sinusoidal distribution of MMFs, ignoring the effect of iron loss and saturation, etc, the induction motor can be modeled in stationary reference frame and synchronously rotating reference frame.

##### 2.2.1 Stationary Two-Axis Model

A 3-phase induction motor has three coils in the rotor and three coils in the stator. The rotor coils are rotating with an electrical angular velocity  $\omega_r$ . The three-phase winding and

their orientation are shown in Fig. 2.1. It appears that the coupling between the stator and rotor coils is a function of position of the rotor and is continuously variable. So it is not wise to model an induction motor using its physical windings. The variables of an induction motor are phases and it can be modeled by equivalent two windings in lieu of three. In this consideration, three stationary stator windings may easily be represented by two equivalent stationary windings. To avoid the complexity of variable coupling, two equivalent stationary windings are considered for rotor circuit. Fig. 2.2 shows the mutually perpendicular fictitious coils of the three-phase equivalent of induction motor. In this connection, voltages due to rotor speed are duly considered. In the mutually perpendicular frame, there is no coupling between the axes quantities, which results in a simple system. Considering the voltage drops in the stator due to resistance, self and mutual inductances, the stator circuit equations are written. In addition to these the speed voltage terms are considered for rotor circuit only. The stator and rotor circuit voltage equations of an induction motor are given in (2.1). Well judged assumptions of no saturation, sinusoidal distribution of flux and mmf and ignoring the effect of iron loss results this set of equations. The stationary axes are indicated as  $\alpha$  and  $\beta$  [30, 31]:

$$\begin{bmatrix} v_{\alpha s} \\ v_{\beta s} \\ 0 \\ 0 \end{bmatrix} = \begin{bmatrix} R_s + L_s p & 0 & L_m p & 0 \\ 0 & R_s + L_s p & 0 & L_m p \\ L_m p & L_m \omega_r & R_r + L_r p & L_r \omega_r \\ -L_m \omega_r & L_m p & -L_r \omega_r & R_r + L_r p \end{bmatrix} \begin{bmatrix} i_{\alpha s} \\ i_{\beta s} \\ i_{\alpha r} \\ i_{\beta r} \end{bmatrix} \quad (2.1)$$

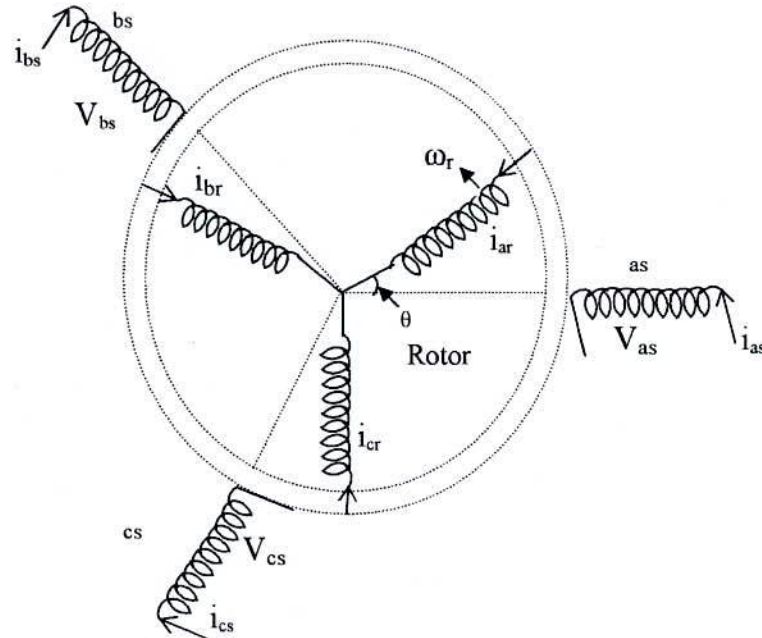


Figure 2.1 Physical Coil system of the stator and the rotor of a 3-phase induction motor.



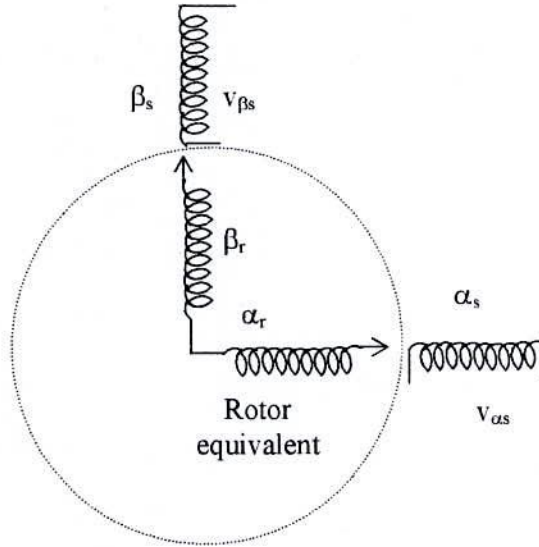


Figure 2.2 Mutually perpendicular fictitious coils of the 3-phase equivalent of induction motor.

The developed electro-magnetic torque of an induction motor of  $P_p$  -pole pairs is:

$$T_e = \frac{3}{2} P_p (i_{\alpha r} [L_m i_{\beta s} + L_r i_{\beta r}] - i_{\beta r} [L_m i_{\alpha s} + L_r i_{\alpha r}]) \quad (2.2)$$

In terms of stator current and stator flux the equation (2.2) can be expressed as:

$$T_e = \frac{3}{2} P_p (\psi_{\alpha s} i_{\beta s} - \psi_{\beta s} i_{\alpha s}) \quad (2.3)$$

where,

$$\bar{\psi}_s = L_s \bar{i}_s + L_m \bar{i}_r \quad (2.4a)$$

$$\bar{\psi}_r = L_r \bar{i}_r + L_m \bar{i}_s \quad (2.4b)$$

$\bar{i}_s = [i_{\alpha s} \ i_{\beta s}]^T$  and  $\bar{i}_r = [i_{\alpha r} \ i_{\beta r}]^T$  are the stator flux, the rotor flux, the stator current and the rotor current vectors respectively.

And the torque balance equation is

$$T_e = J \frac{d\omega_m}{dt} + B\omega_m + T_L \quad (2.5)$$

Where,  $\omega_m = \frac{\omega_r}{P_p}$

### 2.2.2 Synchronously Rotating Two-Axis Model

It is well known that the flux and mmf of an induction motor are synchronously rotating. To visualize the phenomenon of torque production and performance of the induction motor the synchronously rotating mutually perpendicular axes system is considered. This model is also suitable for current fed inverter-coupled system. According to two-axis machine

theory, when a symmetrical induction motor is described in a reference frame that rotates in synchronism with the stator mmf, all the ac phase-variable sets get transformed into equivalent dc variables. Under the usual assumptions of no hysteresis, eddy currents, space harmonics, etc., the basic system of equations of an induction motor in terms of a 2-phase model (d-q variables) in an arbitrary synchronous reference frame is given by [30]:

$$\begin{bmatrix} v_{ds} \\ v_{qs} \\ 0 \\ 0 \end{bmatrix} = \begin{bmatrix} R_s + pL_s & -\omega_e L_s & pL_m & -L_m \omega_e \\ \omega_e L_s & R_s + pL_s & L_m \omega_e & pL_m \\ pL_m & -L_m \omega_{sl} & R_r + pL_r & -L_r \omega_{sl} \\ L_m \omega_{sl} & pL_m & L_r \omega_{sl} & R_r + pL_r \end{bmatrix} \begin{bmatrix} i_{ds} \\ i_{qs} \\ i_{dr} \\ i_{qr} \end{bmatrix} \quad (2.6)$$

Fig. 2.3 shows the spatial relationship between the axes of different frames of reference viz. stator-fixed, rotor-fixed, and synchronously rotating d-q reference frames.

The developed electromagnetic torque is:

$$T_e = \frac{3}{2} P_p L_m (i_{qs} i_{dr} - i_{ds} i_{qr}) \quad (2.7)$$

Equation (2.6) and equation (2.7) can be rearranged as follows:

$$\bar{v}_s^s = R_s \bar{i}_s^s + \frac{d}{dt} \bar{\psi}_s^s + j\omega_e \bar{\psi}_s^s \quad (2.8a)$$

$$0 = R_r \bar{i}_r^s + \frac{d}{dt} \bar{\psi}_r^s + j\omega_{sl} \bar{\psi}_r^s \quad (2.8b)$$

$$T_e = \frac{3}{2} P_p (\psi_{ds} i_{qs} - \psi_{qs} i_{ds}) \quad (2.9)$$

Where,

$$\bar{\psi}_s^s = L_s \bar{i}_s^s + L_m \bar{i}_r^s \quad (2.10a)$$

$$\bar{\psi}_r^s = L_r \bar{i}_r^s + L_m \bar{i}_s^s \quad (2.10b)$$

and  $\bar{v}_s^s = [v_{ds} \ v_{qs}]^T$  is the stator voltage vector,  $\bar{i}_s^s = [i_{ds} \ i_{qs}]^T$  and  $\bar{i}_r^s = [i_{dr} \ i_{qr}]^T$  are the stator and rotor current vectors,  $\omega_e$  is the speed of the synchronous reference frame,  $\omega_{sl}$  is the slip speed,  $R_s$ ,  $R_r$  are the stator and rotor resistances, and  $\bar{\psi}_s^s = [\psi_{ds} \ \psi_{qs}]^T$  and  $\bar{\psi}_r^s = [\psi_{dr} \ \psi_{qr}]^T$  are the stator and rotor flux linkage vectors respectively. The superscript  $s$  in the above equations denotes that the quantity is referred to the synchronous reference frame. Here, the variables  $[\psi_{ds} \ \psi_{qs}]$  and  $[\psi_{dr} \ \psi_{qr}]$  imply the flux linkages with the stator and rotor circuits along the synchronously rotating d- and q-axis respectively.

With reference to Fig. 2.4 if  $i_s$  is the magnitude of the vector current  $\bar{I}_s$ , the corresponding d- and q-axis currents in the synchronous reference frame are:

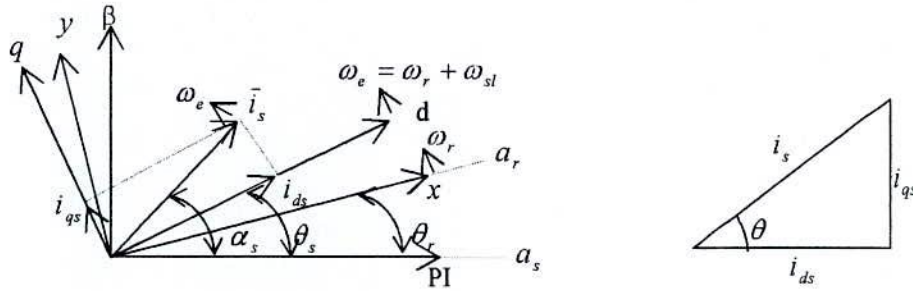
$$\begin{aligned} i_{ds} &= i_s g_{ds} \\ i_{qs} &= i_s g_{qs} \end{aligned} \quad (2.11)$$

Where

$$g_{ds} = \cos\theta$$

$$g_{qs} = \sin \theta$$

$$\tan \theta = \frac{i_{qs}}{i_{ds}} \quad (2.12)$$



- $a_s$  - Actual stator a phase axis
- $a_r$  - Actual rotor a phase axis
- $\alpha - \beta$  - Stator fixed reference frame
- $x - y$  - Rotor fixed reference frame
- $d - q$  - Synchronously rotating reference frame
- $\bar{i}_s$  - Stator mmf vector

Figure 2.3 Relation between various co-ordinate systems and principle of field orientation.

### 2.3 Phase Relationship

- 1) The physical phasors and the fictitious two-axis phasors are shown in Fig. 2.4. Considering the voltages in the axes systems, the relationship among them is established as:

$$v_{\alpha s} = v_a - \frac{1}{2}v_b - \frac{1}{2}v_c$$

$$v_{\beta s} = -\frac{\sqrt{3}}{2}v_b + \frac{\sqrt{3}}{2}v_c \quad (2.13)$$

Similar relationship exists between the currents.

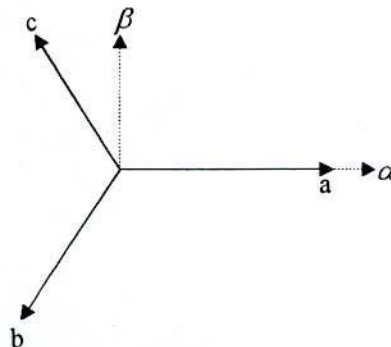


Figure 2.4 Physical 3-phase variables and their equivalent fictitious two-axis phasors.

## 2.4 Induction Motor Model in terms of Stator Current and Rotor Flux

In a speed controlled induction motor drive the motor is fed from a three-phase inverter. The inverter output voltage and current are controlled in a number of ways. The PWM method uses a number of positive and negative pulses per half cycle to control the magnitude and frequency of fundamental component of ac voltage. The simplest inverter generates square voltages at the output. From equation (2.1) and equation (2.2), the basic circuit equations in the stationary reference frame of induction machine can be written as:

$$\begin{bmatrix} \bar{v}_s \\ 0 \end{bmatrix} = \begin{bmatrix} (R_s + pL_s)I & pL_m I \\ pL_m I - \omega_r L_m J & (R_r + pL_r)I - L_r \omega_r J \end{bmatrix} \begin{bmatrix} \bar{i}_s \\ \bar{i}_r \end{bmatrix} \quad (2.14)$$

$$\text{and } T_e = \frac{3}{2} P_p (i_{cr} \psi_{\beta r} + i_{\beta r} \psi_{cr}) \quad (2.15)$$

$$\text{where, } \bar{\psi}_r = L_m \bar{i}_s + L_r \bar{i}_r \quad (2.16)$$

where,  $p \equiv \frac{d}{dt}$  is the time derivative.

The state and output equations are easily derived from equations (2.14) and (2.16) as:

$$\frac{d}{dt} \begin{bmatrix} \bar{i}_s \\ \bar{\psi}_r \end{bmatrix} = \begin{bmatrix} A_{11} & A_{12} \\ A_{21} & A_{22} \end{bmatrix} \begin{bmatrix} \bar{i}_s \\ \bar{\psi}_r \end{bmatrix} + \begin{bmatrix} B_1 \\ 0 \end{bmatrix} \bar{v}_s \quad (2.17)$$

$$\bar{i}_s = \begin{bmatrix} I & 0 \end{bmatrix} \begin{bmatrix} \bar{i}_s \\ \bar{\psi}_r \end{bmatrix} \quad (2.18)$$

Where,

$$A_{11} = - \left\{ \frac{R_s}{\sigma L_s} + R_r \frac{(1 - \sigma^2)}{\sigma L_r} \right\} I$$

$$A_{12} = \frac{L_m}{\sigma L_s L_r} \left\{ \frac{R_r}{L_r} \right\} I - \omega_r J$$

$$A_{21} = \frac{L_m R_r}{L_r} I$$

$$A_{22} = - \frac{R_r}{L_r} I + \omega_r J$$

$$B_1 = \frac{1}{\sigma L_s} I$$

$$I = \begin{bmatrix} 1 & 0 \\ 0 & 1 \end{bmatrix}, \quad J = \begin{bmatrix} 0 & -1 \\ 1 & 0 \end{bmatrix} \quad (2.19)$$

$$\sigma = 1 - \left( \frac{L_m^2}{L_s L_r} \right); \text{ leakage coefficient} \quad (2.20)$$



The state variables are the primary current  $\bar{i}_s = [i_{\alpha s} \ i_{\beta s}]^T$  and the rotor flux  $\bar{\psi}_r = [\psi_{\alpha r} \ \psi_{\beta r}]^T$ . The input is the primary voltage  $\bar{v}_s = [v_{\alpha s} \ v_{\beta s}]^T$ .

## 2.5 Induction Motor Model under Field Orientation Principle

From (2.6) and (2.5) the fifth order non-linear state space model of induction motor is represented in the synchronous reference frame (d-q) as follows:

$$v_{ds} = (R_s + pL_s)i_{ds} - \omega_e L_s i_{qs} + pL_m i_{dr} - \omega_e L_m i_{qr} \quad (2.21)$$

$$v_{qs} = \omega_e L_s i_{ds} + (R_s + pL_s)i_{qs} + \omega_e L_m i_{dr} + pL_m i_{qr} \quad (2.22)$$

$$0 = pL_m i_{ds} - \omega_{sl} L_m i_{qs} + (R_r + pL_r)i_{dr} - \omega_{sl} L_r i_{qr} \quad (2.23)$$

$$0 = \omega_{sl} L_m i_{ds} + pL_m i_{qs} + (R_r + pL_r)i_{qr} + \omega_{sl} L_r i_{dr} \quad (2.24)$$

$$T_e = Jp\omega_m + B\omega_m + T_L \quad (2.25)$$

Where  $\omega_e$ ,  $\omega_r$  and  $\omega_{sl}(=\omega_e - \omega_r)$  are the synchronous, rotor and slip angular speeds respectively and  $L_m$  is the mutual inductance.

From (2.7) the developed electromagnetic torque in terms of  $d$ - and  $q$ - axes components is given by:

$$T_e = \frac{3}{2} P_p L_m (i_{qs} i_{dr} - i_{ds} i_{qr}) \quad (2.26)$$

Where,  $P_p$  is the number of pole pairs.

Components of rotor flux are:

$$\psi_{dr} = L_r i_{dr} + L_m i_{ds} \quad (2.27)$$

$$\psi_{qr} = L_r i_{qr} + L_m i_{qs} \quad (2.28)$$

From (2.27) and (2.28),  $d$ - and  $q$ - axes rotor currents are:

$$i_{dr} = \frac{1}{L_r} (\psi_{dr} - L_m i_{ds}) \quad (2.29)$$

$$i_{qr} = \frac{1}{L_r} (\psi_{qr} - L_m i_{qs}) \quad (2.30)$$

Substituting (2.27)-(2.30) into (2.23) and (2.24) yields:

$$\frac{d\psi_{dr}}{dt} + \frac{R_r}{L_r} \psi_{dr} - \frac{L_m}{L_r} R_r i_{ds} - \omega_{sl} \psi_{qr} = 0 \quad (2.31)$$

$$\frac{d\psi_{qr}}{dt} + \frac{R_r}{L_r} \psi_{qr} - \frac{L_m}{L_r} R_r i_{qs} + \omega_{sl} \psi_{dr} = 0 \quad (2.32)$$

If the field orientation is established such that  $q$ -axis rotor flux is set zero, and  $d$ -axis rotor flux is maintained constant then equations (2.31), (2.32), (2.29), (2.30) and (2.26) becomes:

$$\psi_{dr} = L_m i_{ds} \quad (2.33)$$

$$\omega_{sl} = \frac{1}{\tau_r} \frac{i_{qs}}{i_{ds}} \quad (2.34)$$

$$i_{dr} = 0 \quad (2.35)$$

$$i_{qr} = -\frac{L_m}{L_r} i_{qs} \quad (2.36)$$

$$T_e = \frac{3}{2} P_p \frac{L_m}{L_r} \psi_{dr} i_{qs} \quad (2.37)$$

Where  $\tau_r (= L_r / R_r)$  is the time constant of the rotor. Hence, only  $q$ -axis stator current controls the developed electromagnetic torque.

## 2.6 Analysis of Magnetization Characteristics

The stator and rotor of polyphase induction motors are built with high grade laminated sheets and constitute the magnetic circuit of the polyphase induction motor. A small uniform air gap separates the stator and rotor cores. The magnetic cores exhibit almost linear characteristic at the beginning of the magnetization curve and after the knee point saturation influences the characteristics to be nonlinear drastically. A proper magnetic model of the machine is required to have an exact idea about the performance of the IM drives. From the experimental data the true magnetization characteristic can be evaluated [32]. If  $V_s$  be the applied rms voltage to an IM, the mutual flux linkage can be written as:

$$\psi_m = \frac{\sqrt{2}V_s}{\omega_e} \quad (2.38)$$

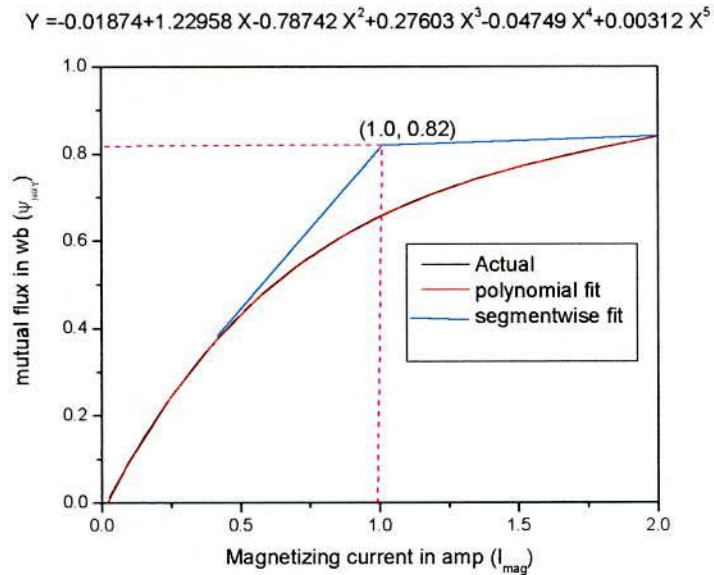
To obtain information on (2.38) for the motors, whose nominal parameters are furnished in Appendix I and the test were performed in the laboratory. The machine under test was driven at synchronous speed by an auxiliary motor and the stator was supplied from a constant frequency variable voltage source. From the recorded ammeter, voltmeter and wattmeter data after subtracting the stator resistance and leakage-reactance drops, the deduced true saturation characteristic and its magnetizing inductance are shown in Fig. 2.5(a) and 2.5(b) respectively. The leakage flux of the induction motor is only a small percentage of the mutual flux and does not vary too much due to saturation effect [33]. From the fitted curve the equations of mutual flux linkage and mutual inductance are:

$$\psi_{mag} = a_0 + a_1 i_{mag} + a_2 i_{mag}^2 + a_3 i_{mag}^3 + a_4 i_{mag}^4 + a_5 i_{mag}^5 \quad (2.44)$$

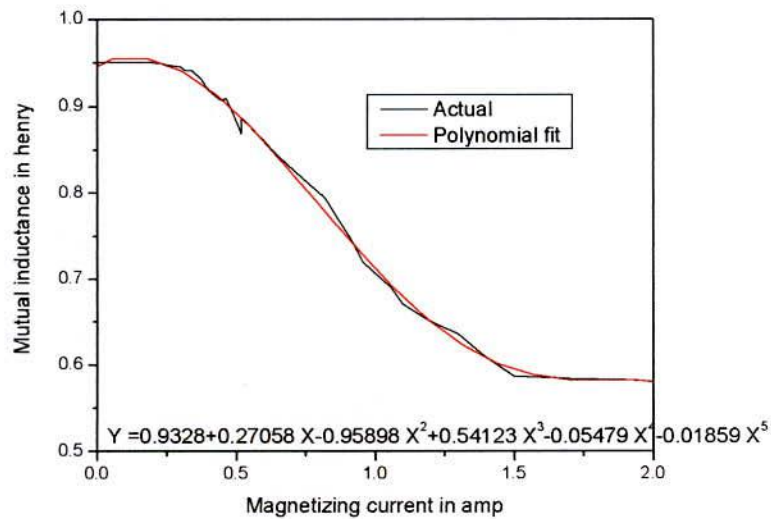
$$L_m = b_0 + b_1 i_{mag} + b_2 i_{mag}^2 + b_3 i_{mag}^3 + b_4 i_{mag}^4 + b_5 i_{mag}^5 \quad (2.45)$$

The coefficients  $a$  s and  $b$  s of the above equations are indicated in the corresponding figures in 2.5(a) and 2.5(b), respectively. Segmentwise linear characteristics are sometimes

promising for easier analysis of the induction machine and it is imposed for Fig. 2.5(a) as indicated. Here two segment linear characteristic is considered and the approximate characteristic is used to find out the knee point of the magnetization characteristic. This point is used to find out  $\psi_{mo}$  and  $I_{mo}$  as the parameters of the knee point. Up to the knee point starting from the origin the mutual inductance  $L_m$  is assumed to have constant value.



(a)



(b)

Figure 2.5 Magnetization characteristics (a) true saturation characteristic and (b) magnetizing inductance

## **2.7 Conclusion**

In this chapter the induction motor model in arbitrary reference frame is discussed in detail. A dynamic model of the machine subjected to control must be known in order to understand and design high performance controlled drives. The condition to achieve field orientation control is derived. Magnetic saturation in induction motor drive is considered for more realistic representation in the analysis. The magnetic saturation is incorporated in the machine model as a variable magnetizing inductance.



## CHAPTER III

### QEA and Fast Speed Response IM Drive

#### 3.1 Introduction

Selection of controller parameters is a challenge for researchers in high performance drives. Specially, to produce required variable dynamics from the drive system Proportional-Integral (PI) controller constants may be obtained using on line tuning through genetic or evolutionary algorithms. There are different evolutionary algorithms such as Evolution Strategies, Evolutionary programming, Genetic Algorithm (GA), Particle Swarm Optimization (PSO), Differential Evolution (DE) etc. and these are called Conventional Genetic Algorithm (CGA).

Quantum Evolutionary Algorithm (QEA) is a novel probability optimization algorithm based on the concept and principles of quantum computing [14]. Instead of binary, numeric or symbolic representation, QEA uses quantum bit or Q-bit. Compared with Conventional Genetic Algorithm (CGA), QEA has a better characteristic of diversity in the population and can keep the balance of exploration and exploitation more easily- even with a small population. So QEA has become a research hotspot in recent years.

In this chapter, QEA is used to select the gain coefficients of PI controllers in the proposed control system. A comparative analysis between QEA and CGA based control system has been done here.

#### 3.2 Conventional Genetic Algorithm (CGA)

Producing initial populations is the first step of CGA. The population is composed of the chromosomes that are binary bit stream or real codes. The corresponding evaluation of a population is called the fitness function. It is the performance index of a population. In this project the fitness function is defined as

$$F = (\omega_{ref} - \omega_r)^2 \quad (3.1)$$

The evolution procedure of CGA is shown in Fig. 3.1. The overshoot and settling time of the controlled system is used as the performance index of fitness function. Then fitness function [34] can be defined as  $F = f_1 \times f_2$ . The definitions of  $f_1$  and  $f_2$  are  $f_1 = e^{-(OT/K_I)^2}$ ,  $f_2 = e^{-(ST/K_P)^2}$  where  $OT$  is the overshoot time quantity and  $ST$  is the settling time quantity.  $K_I$  and  $K_P$  are weight factors that control the value of overshoot and settling time.

After the fitness function is calculated, the fitness value and the number of the generation determine whether the evolution procedure is stopped or not. In the following, the new populations are generated through reproduction, crossover, and mutation.

Reproduction is a process to decide how many copies of individuals strings should be produced in the mating pool according to their fitness value. The reproduction operation allows strings with higher fitness value to have larger number of population while the strings with lower fitness values have a relatively smaller number of copies or even none at

all. The selection operation decides which parents take part in reproducing offspring for the next generation.

Crossover is a recombined operator for two high-fitness strings (parents) to produce two off springs by matching their desirable quantities through a random process. The crossover operation is applied to generate new chromosomes. The equations of the new populations generated from crossover are [34]

$$x_{01} = (1 - \alpha)x_{p1} + \alpha x_{p2} \quad (3.2)$$

$$x_{02} = (1 - \alpha)x_{p2} + \alpha x_{p1} \quad (3.3)$$

Where  $x_{p1}$  and  $x_{p2}$  are the old chromosomes,  $\alpha$  is the random value from 0 to 1,  $x_{01}$  and  $x_{02}$  are the new chromosomes.

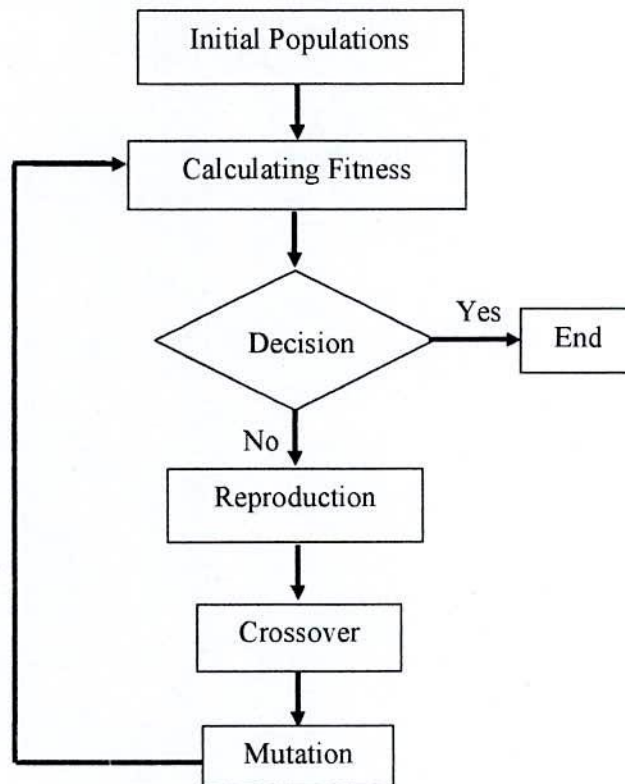


Figure 3.1 Evolution Procedure of CGA.

Mutation is a method to find the global optimum value. It is a process to provide an occasional random alternation of the value at a particular string position. In the project, Time Variant Mutation (TVM) operator is used to mutate all variables of offspring [34]. It is ought to be taken care that initially this type of mutation might violate the domain of the object variables. In case of domain violations for any offspring, that offspring is left without mutation.

In this thesis work, CGA is used to optimize the gains of PI controller in the speed loop of the control system for comparing with the performance of the proposed QEA based control system. Parameters used in CGA are given below:

Population size=20; Crossover Probability= [0 to 1] Selected from united random number; Mutation Probability=0.4; No. of Generation=100.

### 3.3 Quantum Evolutionary Algorithm (QEA)

The QEA is a stochastic search and optimization method based on the principles of natural biological evolution such as the quantum bit and the superposition of states [14]. The QEA can treat the balance between exploration and exploitation more easily when compared with CGA. Producing initial populations is the first step of QEA. The population is composed of the chromosomes that are represented by quantum bit or Q-bit which is the smallest unit of information in QEA. The corresponding evaluation of a population is called the fitness function. It is the performance index of a population. In this project, the fitness function is defined as:

$$Fitness = \frac{1}{\zeta + 1} \quad (3.4)$$

Where,  $\zeta = \int |speed\_error| dt$  is the objective function and  $speed\_error = \omega_m^* - \omega_m$ .

#### 3.3.1 Representation of QEA

A number of different representations can be used to encode the solutions onto individuals in evolutionary computation. The representations can be classified broadly as: binary, numeric, and symbolic. QEA uses a new representation, called a Q-bit, for the probabilistic representation that is based on the concept of qubits, and a Q-bit individual as a string of Q-bits.

A Q-bit may be in the 1 state, in the 0 state, or in any superposition of the two. Superposition of logical state can be expressed as  $\alpha|0\rangle + \beta|1\rangle$ . Another way of writing superposition as a vector is shown below:

$$\alpha|0\rangle + \beta|1\rangle \leftrightarrow \begin{pmatrix} \alpha \\ \beta \end{pmatrix} \quad (3.5)$$

The complex numbers  $\alpha$  and  $\beta$  are called the amplitudes of the superposition.  $|\alpha_i|^2$  gives the probability that the Q-bit will be found in 0 state and  $|\beta_i|^2$  gives the probability that the qubit will be found in 1 and they satisfy the normalization condition  $|\alpha_i|^2 + |\beta_i|^2 = 1$ . A Q-bit is also defined with a pair of numbers  $(\alpha, \beta)$  and a Q-bit individual as a string of  $m$  Q-bits is defined as [14]:

$$q = \begin{bmatrix} \alpha_1 & \alpha_2 & \dots & \alpha_m \\ \beta_1 & \beta_2 & \dots & \beta_m \end{bmatrix} \quad (3.6)$$

Where  $|\alpha_i|^2 + |\beta_i|^2 = 1, i = 1, 2, 3 \dots m$ . A Q-gate defined as a mutation operator is applied on the Q-bit to update their probability amplitudes as follows:

$$\begin{pmatrix} \alpha'_i \\ \beta'_i \end{pmatrix} = \begin{bmatrix} \cos(\Delta\theta_i) & -\sin(\Delta\theta_i) \\ \sin(\Delta\theta_i) & \cos(\Delta\theta_i) \end{bmatrix} \begin{pmatrix} \alpha_i \\ \beta_i \end{pmatrix} \quad (3.7)$$

Where  $\Delta\theta_i$ ,  $i=1, 2, 3 \dots, m$ , is the rotation angle of a Q-bit towards the 0 state or 1 state depending on its sign.  $|\alpha_i|$  and  $|\beta_i|$  must satisfy the normalization condition  $|\alpha_i|^2 + |\beta_i|^2 = 1$ . The crossover operator is employed after a given interval of generations. Along with Q-bit population, a binary population is also maintained for evaluation process.

### 3.3.2 Procedure of QEA

```

begin
     $t \leftarrow 0$ 
    initialize  $Q(t)$ 
    make  $P(t)$  by observing  $Q(t)$  states
    evaluate  $p(t)$ 
    store the best solution among  $P(t)$ 
while (not termination-condition) do
    begin
         $t \leftarrow t+1$ 
        make  $P(t)$  by observing  $Q(t-1)$  states
        evaluate  $p(t)$ 
        update  $Q(t)$  using quantum gates  $U(t)$ 
        store the best solution among  $P(t)$ 
    end
end

```

Where  $Q(t)$  is a population of qubit chromosomes at generation  $t$ , and  $P(t)$  is a set of binary solutions at generation  $t$ .

In the step of initialize  $Q(t)$ , all qubit chromosomes are initialized with the same constant. It means that one qubit chromosome represents the linear superposition of all possible states with the same probability. The next step makes a set of binary solutions,  $P(t)$ , by observing  $Q(t)$  states. One binary solution is formed by selecting each bit using the probability of qubit. And then each solution is evaluated to give some measure of its fitness. The initial best solution is then selected and stored among the binary solutions,  $P(t)$ .

In the **while** loop, one more step, update  $Q(t)$ , is included to have fitter states of the qubit chromosomes. A set of binary solutions,  $P(t)$ , is formed by observing  $Q(t-1)$  states as with the procedure described before, and each binary solution is evaluated to give the fitness value. In the next step, update  $Q(t)$ , a set of qubit chromosomes  $Q(t)$  is updated by applying some appropriate quantum gates  $U(t)$ , which is formed by using the binary solutions  $P(t)$  and the stored best solution. The appropriate quantum gates can be designed in compliance with practical problems. Rotation gate is used as a basic gate of QEA. This step makes the qubit chromosomes converge to the fitter states. The best solution among

$P(t)$  is selected in the next step, and if the solution is fitter than the stored best solution, the stored solution is replaced by the new one. The binary solutions  $P(t)$  are discarded at the end of the loop. In the project, QEA is used to optimize the value of two gains  $k_p$  and  $k_i$ .

The overall structure of QEA is shown in Fig. 3.2.

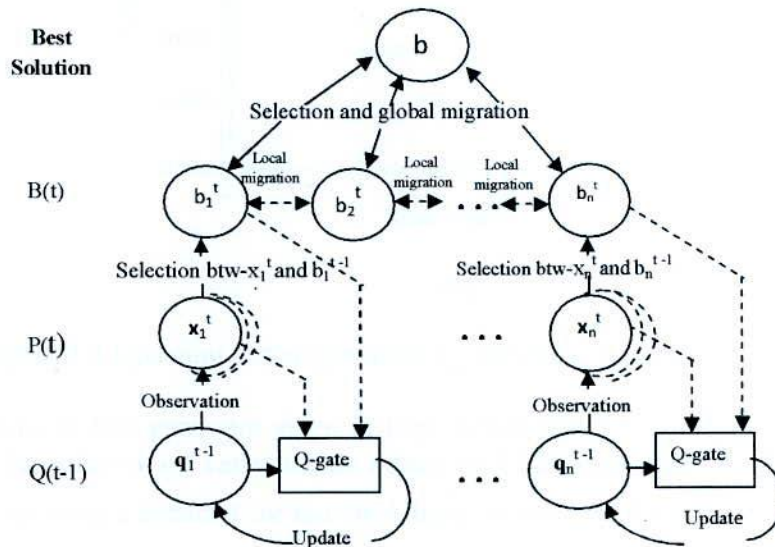
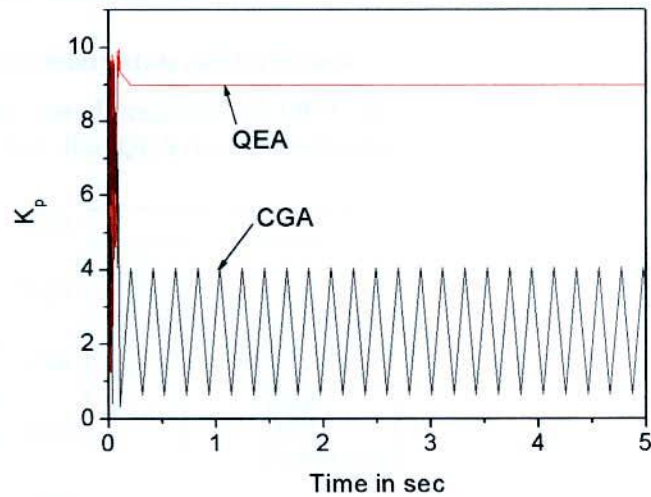


Figure 3.2 Overall structure of QEA [14].



(a)

reference value (125 rad/s) faster than that of CGA controller. Similar characteristic was shown when the reference speed was changed from 125 rad/s (1193.5 rpm) to 75 rad/s (716 rpm). The faster speed response would be clear from Fig. 3.5 which is the small scale representation of Fig. 3.4 into two parts, one is transient condition and the other is steady state condition. From Fig. 3.5(a), it can be seen that settling time for CGA based PI controller is 0.49 sec. whereas that of QEA based PI controller is 0.41 sec. when reference speed was chosen 125 rad/s. Fig. 3.5(b) shows the speed response fluctuation at steady state condition in case of CGA controller whereas that of QEA controller is almost constant.

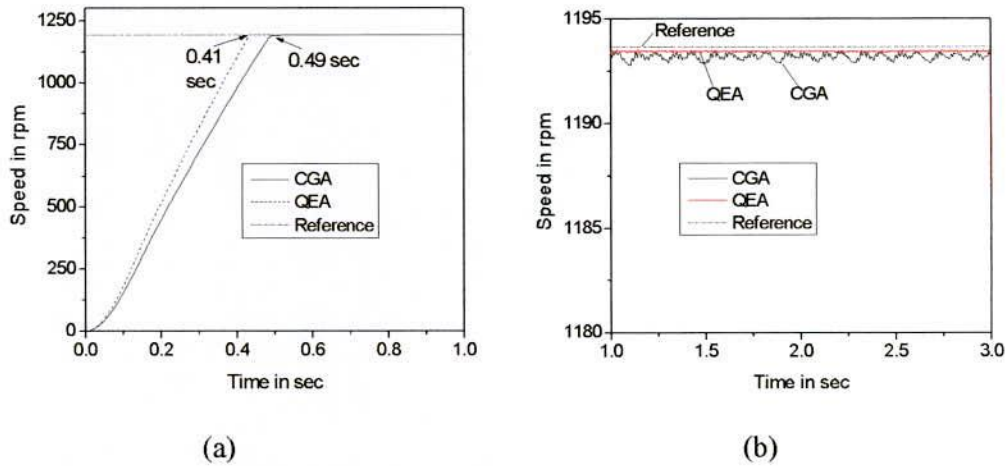


Figure 3.5 Zoomed Speed response of QEA and CGA based PI controller at (a) Transient condition for the time 0 to 1sec. (b) Steady state condition for the time 1 sec. to 3 sec. of Fig. 3.4.

### 3.4.2 Fast Speed Response IM Drive

Fast speed response of another induction motor with different rating is further achieved using QEA based PI controller tuning compared with CGA based PI controller tuning and shown in Fig. 3.6. Effectiveness of the controller is also tested by different set speed. It is observed that QEA based system needs 0.24 sec. to speed up the motor at reference speed 1500 rpm whereas CGA based system needs 0.27 sec.

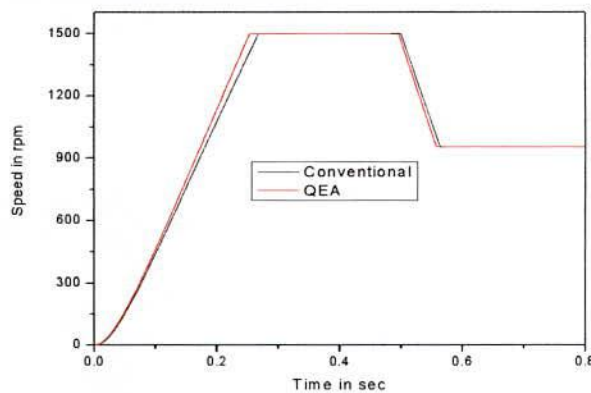


Figure 3.6 Speed response of IM drive using conventional PI controller and QEA based PI controller with different set speed.

### 3.5 Conclusion

In this chapter, a quantum evolutionary algorithm (QEA) based PI controller has been used to replace the conventional genetic algorithm (CGA) based PI controller in the control system of induction motor drive. As the representation style of QEA is Q-bit, it can store more state as well as the searching area is more compared to CGA with same number of register and better solution is obtained. Besides this, in CGA the parents are always replaced by offspring whereas in QEA the parents are not always replaced by offspring. The offspring is tested first whether it is better than the parents or not to replace the parents. This is why there are less probability of fluctuation the gain coefficients of PI controller. So, the motor runs smoothly at steady state condition than CGA based control system. It is observed that the proposed QEA based PI controller need less time to speed up the motor at transient condition and generate negligible speed fluctuation at rated speed under steady state condition. The proposed QEA based controller is capable to drive the load smoothly and shows better performance in load disturbance condition. The performance of the controller remarkable and future research industrial applications will find optimization through QEA.

## CHAPTER IV

### Chaotic Learning Based ANN

#### 4.1 Introduction

Chaos theory is a mathematical sub-discipline that studies complex systems that contain so much motion and computers are required to calculate all the various possibilities. The seemingly random events of nonlinear dynamics are actually predictable from simple deterministic equations using chaos. So, the flux of induction motor can be predicted more accurately under steady state and transient conditions using chaos.

The neural networks have become well established in induction motor drive for different tasks especially for estimation of rotor flux. Since the 1990s, several investigations into the applications of neural networks in the field of electrical machines and power electronics have appeared. Using artificial neural networks (ANNs) the rotor flux components of IM can easily be estimated which is insensitive to motor parameter variations. But local minimum is an integrated problem in training of ANNs and the speed of convergence is very slow due to this effect. To avoid this problem, the chaotic variations of learning rate (LR) are included with the conventional learning rate. In this chapter, chaotic variations of LR have been included with the learning rate of three algorithms such as backpropagation (BP), Real Time Recurrent Learning (RTRL) and Correlated Real Time Recurrent Learning (CRTRL) algorithms to estimate the rotor flux components of induction motor drive accurately. All the algorithms mentioned above generate a chaotic time series with logistic map.

#### 4.2 Chaos Variables

The name "chaos theory" comes from the fact that the systems are apparently disordered. It is really about finding the underlying order in apparently random data. Chaos variables are usually generated by the well-known logistic map. The logistic map is a one-dimensional quadratic map defined by:

$$\gamma(k+1) = \mu\gamma(k)(1 - \gamma(k)) \quad (4.1)$$

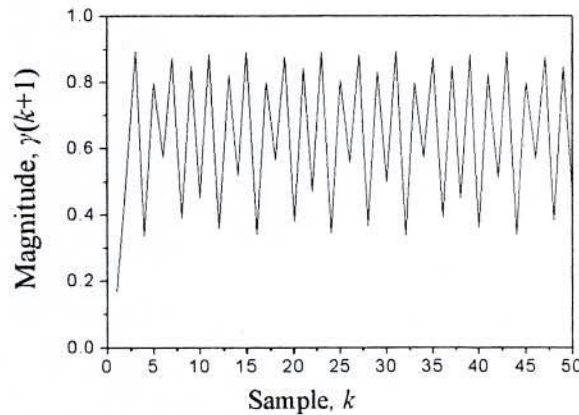


Figure 4.1 The logistic mapping.



Where  $0 \leq \mu \leq 1$  is a control parameter,  $k$  denotes a discrete time step and  $\gamma(k)$  denotes a data at  $k$ . Despite the apparent simplicity of the equation, the solution exhibits a rich variety of behavior. For  $\mu = 3.58 \sim 4.0$ , it generates chaotic evolutions [17]. Its output is like a stochastic output, no value of  $\gamma$  is repeated and the deterministic equation is sensitive to initial conditions as shown in Fig. 4.1. Just a small change in the initial conditions can drastically change the long-term behavior of a system. Such a small amount of difference in a measurement might be considered experimental noise, background noise, or an inaccuracy of the equipment.

### 4.3 Chaotic Learning Based Back-Propagation Algorithm

The most dominant algorithm for pattern recognition is, so far proved, the back-propagation algorithm. It should be mentioned here, for multilayer perceptron (MLP) back-propagation algorithm is widely used [36]. Here, the basic of the back-propagation algorithm with chaotic learning rate is briefly discussed.

The error signal at the output of neuron  $j$  at iteration  $n$  is defined by:

$$e_j(n) = d_j(n) - y_j(n) \quad (4.2)$$

Here, neuron  $j$  is an output node.

The instantaneous value of total error energy can be written as per definition:

$$\varepsilon(n) = \frac{1}{2} \sum_{j \in C} e_j^2(n) \quad (4.3)$$

Where, the set  $C$  includes all the neurons in the output layer of the network. Let  $N$  denotes the total number of patterns contained in the training set. The *average squared error energy*, is obtained by summing  $\varepsilon(n)$  over all  $n$  and then normalizing with respect to the set size  $N$  as represented by:

$$\varepsilon_{av} = \frac{1}{N} \sum_{n=1}^N \varepsilon(n) \quad (4.4)$$

For a given training set,  $\varepsilon_{av}$  represents the *cost function* as a measure of learning performance. The objective of learning process is to adjust the free parameters of the network to minimize  $\varepsilon_{av}$ .

Again, the induced local field  $v_j(n)$  produced at the input of the activation function associated with neuron  $j$  is therefore:

$$v_j(n) = \sum_{i=0}^m w_{ji}(n) y_i(n) \quad (4.5)$$

Where,  $m$  is the total number of inputs (excluding bias) applied to the neuron  $j$ .

The functional signal appearing at the output of neuron  $j$  at iteration  $n$  is:

$$y_j(n) = \varphi_j(v_j(n)) \quad (4.6)$$

The back-propagation algorithm applies a correction  $\Delta w_{ji}(n)$  to the synaptic weight  $w_{ji}(n)$ , which is proportional to the partial derivative  $\partial \varepsilon(n) / \partial w_{ji}(n)$ . According to the chain rule of calculus we may express the gradient as:

$$\frac{\partial \varepsilon(n)}{\partial w_{ji}(n)} = \frac{\partial \varepsilon(n)}{\partial e_j(n)} \frac{\partial e_j(n)}{\partial y_j(n)} \frac{\partial y_j(n)}{\partial v_j(n)} \frac{\partial v_j(n)}{\partial w_{ji}(n)} \quad (4.7)$$

The left term represents a *sensitivity factor*.

Differentiating both side of (4.3) with respect to  $e_j(n)$ , it becomes:

$$\frac{\partial \varepsilon(n)}{\partial e_j(n)} = e_j(n) \quad (4.8)$$

Differentiating both sides of (4.2) with respect to  $y_j(n)$ , it becomes:

$$\frac{\partial e_j(n)}{\partial y_j(n)} = -1 \quad (4.9)$$

Next, Differentiating both side of (4.6) with respect to  $v_j(n)$ , it becomes:

$$\frac{\partial y_j(n)}{\partial v_j(n)} = \varphi_j'(v_j(n)) \quad (4.10)$$

Finally, differentiating (4.5) with respect to  $w_{ji}(n)$  yields:

$$\frac{\partial v_j(n)}{\partial w_{ji}(n)} = y_i(n) \quad (4.11)$$

The use of (4.8) to (4.11) in (4.7) yields:

$$\frac{\partial \varepsilon(n)}{\partial w_{ji}(n)} = -e_j(n) \varphi_j'(v_j(n)) y_i(n) \quad (4.12)$$

The correction is defined by the *delta rule*:

$$\Delta w_{ji}(n) = -(\eta + \gamma) \frac{\partial \varepsilon(n)}{\partial w_{ji}(n)} \quad (4.13)$$

Where,  $\eta$  is the learning rate parameter of the back-propagation algorithm and  $\gamma$  is the chaos variables. Now it can be said chaotic learning based back-propagation algorithm [37]. The minus sign indicates *gradient descent* in weight space. Accordingly, the use of (4.12) in (4.13) yields:

$$\Delta w_{ji}(n) = -(\eta + \gamma) \delta_j(n) y_i(n) \quad (4.14)$$

Where the local gradient  $\delta_j(n)$  is defined by:

$$\begin{aligned} \delta_j(n) &= -\frac{\partial \varepsilon(n)}{\partial v_j(n)} \\ &= -\frac{\partial \varepsilon(n)}{\partial e_j(n)} \frac{\partial e_j(n)}{\partial y_j(n)} \frac{\partial y_j(n)}{\partial v_j(n)} \\ &= e_j(n) \varphi_j'(v_j(n)) \end{aligned} \quad (4.15)$$

The local gradient points to required changes in synaptic weights. According to (4.15) the local gradient  $\delta_j(n)$  for output neuron  $j$  is equal to the product of the corresponding error signal  $e_j(n)$  for that neuron and derivative  $\varphi_j'(v_j(n))$  of the associated activation function.

#### 4.4 RTRL and CRTRL Algorithm for ANN

The RTRL algorithm derives its name from the fact that adjustments are made to the synaptic weights of a fully connected recurrent network in real time. Fig. 4.2 shows the layout of such a recurrent network [36].

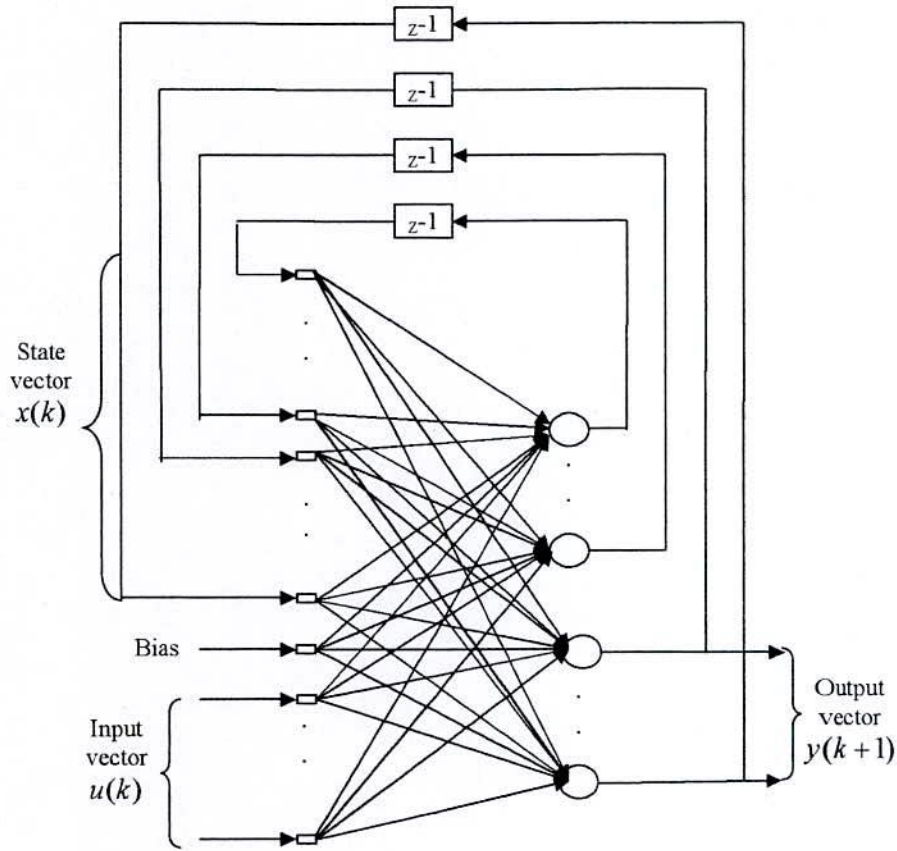


Figure 4.2 Fully connected real time recurrent network

In Mathematical terms, the dynamical behavior of any noise free system can be described by the following pair of nonlinear equations:

$$x(k+1) = \varphi(W_a x(k) + W_b u(k)) \quad (4.16)$$

$$Y(k) = Cx(k) \quad (4.17)$$

Where,  $x(k)$  is the  $q$ -by- $1$  nonlinear state matrix,  $u(k)$  is the  $(m+1)$ -by- $1$  input matrix,  $Y(k)$  is the  $p$ -by- $1$  corresponding output matrix,  $W_a$  is the  $q$ -by- $q$  matrix,  $W_b$  is the  $q$ -by- $(m+1)$  matrix and  $C$  is the  $p$ -by- $q$  matrix.

The process equation (4.16) is reproduced here in the following expanded form:

$$x(k+1) = \begin{bmatrix} \varphi(W_1^T z(k)) \\ \vdots \\ \varphi(W_j^T z(k)) \\ \vdots \\ \varphi(W_q^T z(k)) \end{bmatrix} \quad (4.18)$$

It is assumed that all the neurons have a common activation function  $\varphi(\cdot)$ . The  $(q+m+1)$ -by-1 vector  $w_j$  is the synaptic weight vector of neuron  $j$  in the recurrent network, that is:

$$w_j = \begin{bmatrix} w_{a,j} \\ w_{b,j} \end{bmatrix}, j=1,2 \dots, q \quad (4.19)$$

Where  $w_{a,j}$  and  $w_{b,j}$  are the  $j$ th columns of the transposed weight matrices  $W_a^T$  and  $W_b^T$  respectively. The  $(q+m+1)$ -by-1 vector:

$$Z(k) = \begin{bmatrix} x(k) \\ u(k) \end{bmatrix} \quad (4.20)$$

To simplify the presentation of the RTRL, we define matrices as follows [38]:

The derivative matrix of the  $q$ -by-1 nonlinear state matrix  $x(k)$  with respect to the weight vector  $W_i$ :

$$\Lambda_i(k) = \frac{\partial x(k)}{\partial w_i(k-1)} \quad (4.21)$$

$Z_i(k)$  is a  $q$ -by- $(q+m+1)$  matrix whose rows are all zero, except for the  $i$ th row that is equal to the transpose of vector  $z(k)$ :

$$Z_i(k) = \begin{bmatrix} 0^T \\ z^T(k) \\ 0^T \end{bmatrix} \leftarrow \text{ithrow } i=1,2,\dots,q \quad (4.22)$$

$\varphi(k)$  is a  $q$ -by- $q$  diagonal matrix:

$$\varphi(k+1) = \text{diag} [\varphi'(W_1^T(k)z(k)), \varphi'(W_2^T(k)z(k)), \dots, \dots, \varphi'(W_q^T(k)z(k))] \quad (4.23)$$

With these definitions, the following recursive equation  $\Lambda_i$  for the neuron  $i$  can be obtained by differentiating Eq. (4.21) with respect to  $W_i$  and using the chain rule of calculus:

$$\Lambda_i(k+1) = \varphi(k+1)[W_a(k)\Lambda_i(k) + Z_i(k)] \quad (4.24)$$

The objective of the learning process is to minimize a cost function obtained by the instantaneous sum of squared errors at time  $k$ , which is defined in terms of  $e(k)$  by

$$J(k) = \frac{1}{2} e^T(k)e(k) \quad (4.25)$$

Where the  $p$ -by-1 error vector  $e(k)$  is defined by using the following measurement equation:

$$e(k) = \tilde{y}(k) - y(k) \quad (4.26)$$

Where  $\tilde{y}(k)$  denotes the desired output vector.

The adjustment for the weight vector of the  $i$ th neuron  $\Delta W_i$  is:

$$\Delta W_i(k) = (\eta + \gamma) \frac{\partial J(k)}{\partial W_i(k)} = (\eta + \gamma) C \Lambda_i(k) e(k), \quad i = 1, 2, 3, \dots, q \quad (4.27)$$

Hence, the new weight vector of the  $i$ th neuron is:

$$W_i(k+1) = W_i(k) + \Delta W_i(k) \quad (4.28)$$

Rotor Flux Synthesis by CRTRL Algorithms is shown Fig. 4.3. The difference between RTRL and CRTRL is outputs of CRTRL are correlated whereas RTRL output is uncorrelated to each other.

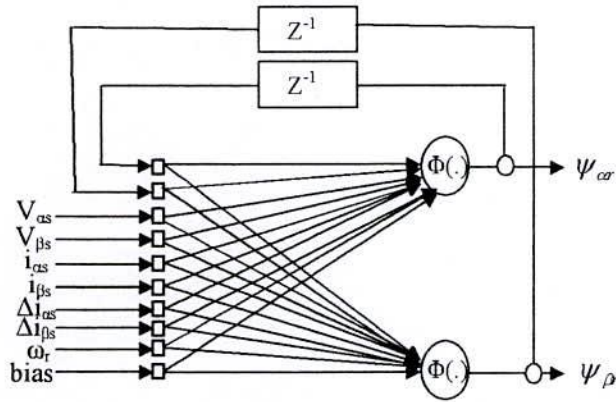
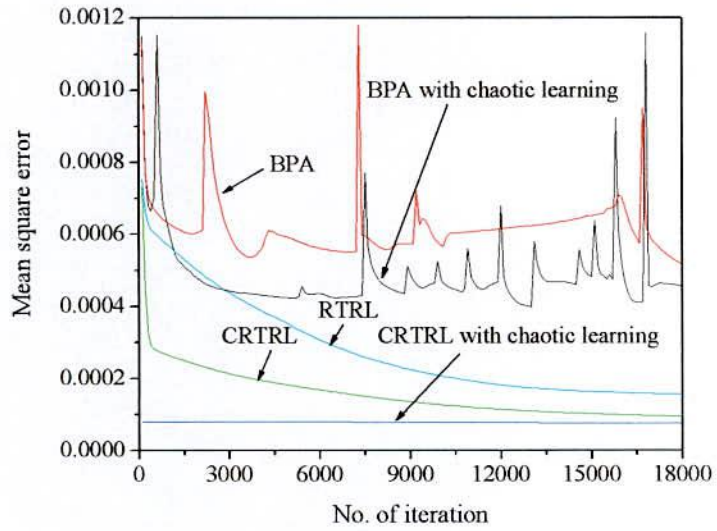
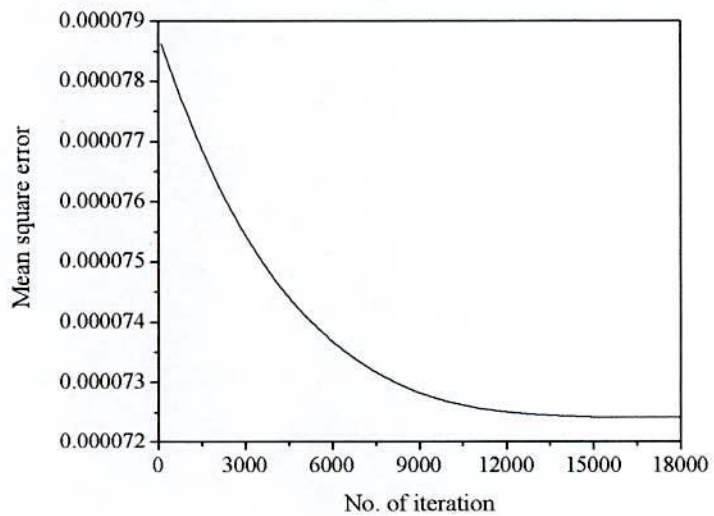


Figure 4.3 Stationary  $\alpha$ - and  $\beta$ - axes rotor flux synthesis by CRTRL algorithm.

The same machine input data are used to train the Back propagation, RTRL, CRTRL, and proposed chaotic learning based CRTRL networks. Both RTRL and CRTRL have no hidden layer whereas the back propagation algorithm required two hidden layers for estimation of rotor flux and the structure of learned back propagation algorithm is 5-8-8-2. Fig. 4.4 shows the comparisons of mean square errors for backpropagation and different RTRL algorithms. From the error data and curves in Fig. 4.4(a), it is clear that the mean square error (MSE) is smaller in the proposed Chaotic Learning based CRTRL algorithm than that of other RTRL algorithms. Hence, proposed chaotic learning based CRTRL estimator is superior to that of Back propagation, RTRL, and CRTRL estimators without chaotic learning rate. To visualize the improvement of chaotic learning based CRTRL by MSE, a small scale representation of mean square error for chaotic learning rate based CRTRL has been shown in Fig. 4.4(b). It is observed that proposed chaotic learning based CRTRL accelerates the weight update into the local minimum zone whereas the constant learning rate based CRTRL is unable to reach. Hence the proposed flux estimator overcomes the problem in training of ANNs. It is also apparent that the rate of convergence of MSE starts after the ending point of conventional constant learning based CRTRL. Numeric improvement of chaotic learning based ANNs have also been shown in Table 4.1.



(a)



(b)

Figure 4.4 (a) Mean square error comparisons between Back-propagation, RTRL and CRTRL algorithms using chaotic learning based ANN (b) Small scale representation of MSE for chaotic learning based CRTRL.

Table 4.1 Mean square error comparison

Back-propagation algorithm	Back-propagation algorithm with chaotic learning	RTRL algorithm	CRTRL algorithm	CRTRL algorithm with chaotic learning
0.00052	0.0004	0.00016	0.00009	0.0000725

#### 4.5 Simulation Results

Simulation studies have been conducted in order to establish the functionality of the proposed estimation scheme. Simulation results for transient and steady state conditions of the field orientation controlled induction motor concerning the proposed chaotic learning based ANN estimators have been presented in this section. In the simulated tests, for comparison purpose, the real or actual flux has been obtained by the voltage flux model described in equations (2.1).

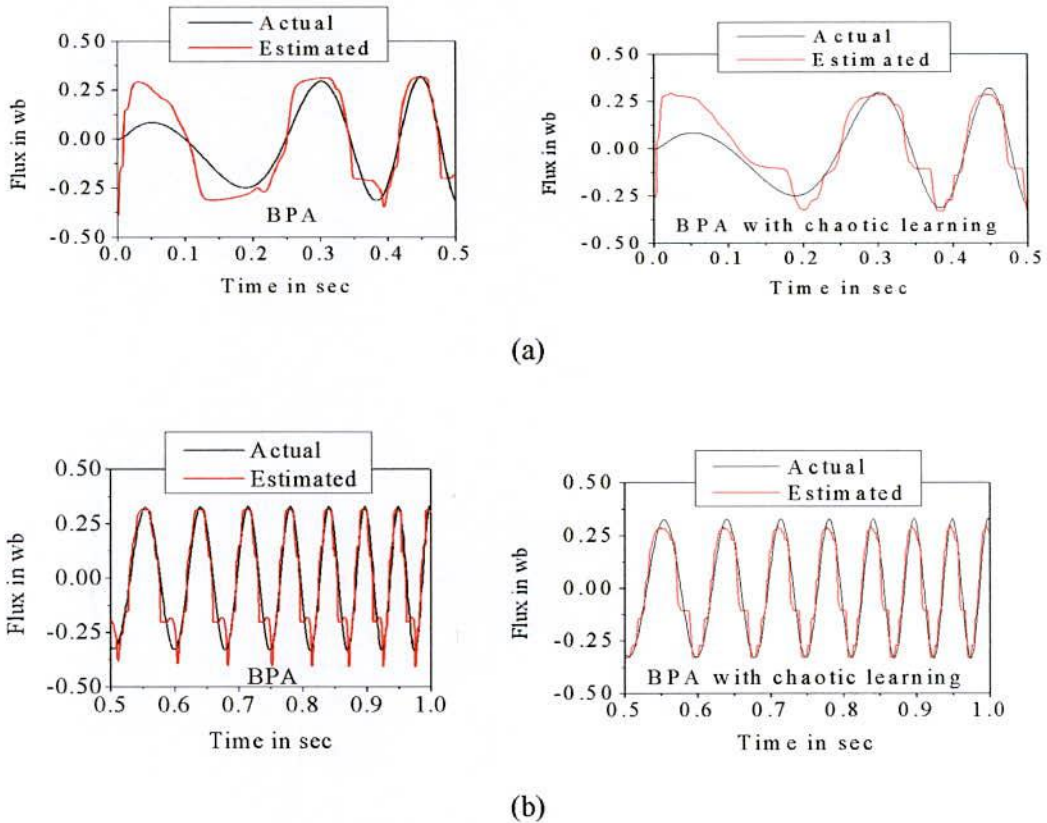
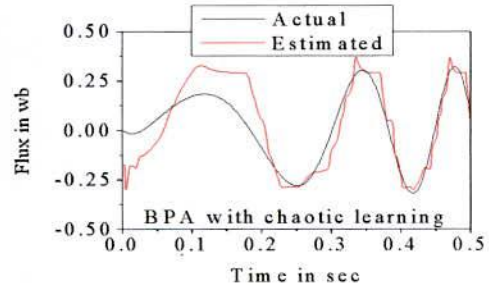
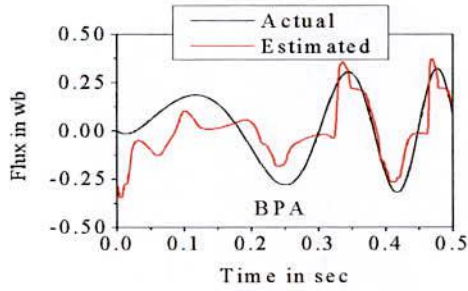
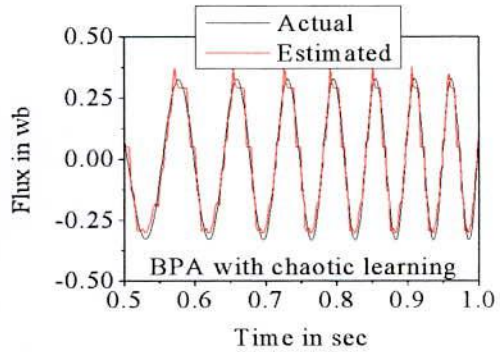
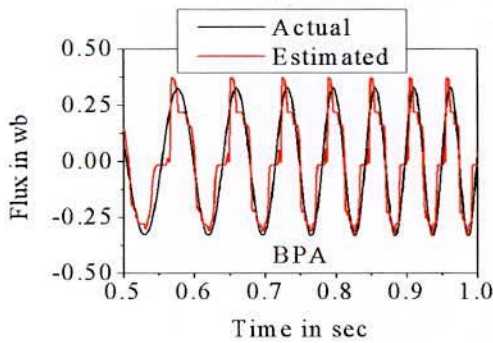


Figure 4.5  $\alpha$ -axis rotor flux estimation using backpropagation algorithm (a) transient and (b) steady state.

Figs. 4.5 and 4.6 show the actual and estimated  $\alpha$ - and  $\beta$ -axes rotor flux respectively at both of transient and steady state conditions using backpropagation algorithm. Without chaotic learning rate, the estimated flux components cannot follow the reference flux precisely. It is found that chaotic learning based backpropagation algorithm is capable to estimate the flux more accurately especially the phase of the reference flux at both of transient and steady state conditions. The amplitude of estimated flux components decreases at transient conditions but it overcome at steady state conditions and shown in the next section. Hence, chaotic learning based backpropagation algorithm shows better performance than without chaotic learning.



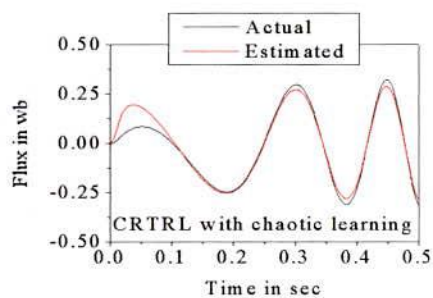
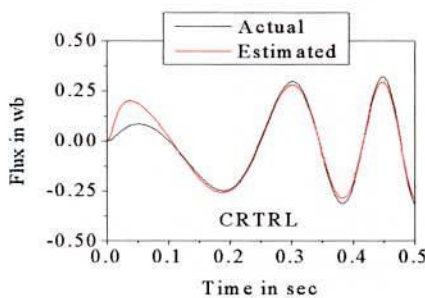
(a)



(b)

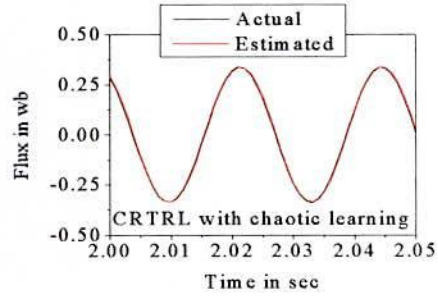
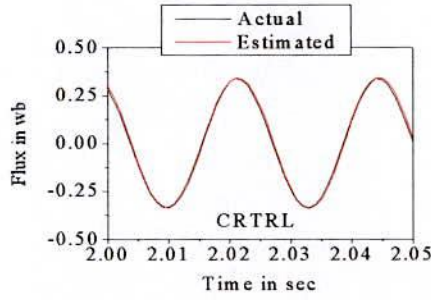
Figure 4.6  $\beta$ -axis rotor flux estimation using BP algorithm (a) transient and, (b) steady state.

Figs. 4.7 and 4.8 show the estimated  $\alpha$ - and  $\beta$ -axes rotor flux respectively with its trained value under both of transient and steady state conditions. The training is performed for CRTRL algorithms. The phase tracking of reference signal is more accurate in both flux components and it is obvious from Fig. 4.8(a). Though the amplitude of estimated flux decreases at transient condition, it overcome at steady state condition and follow the reference flux accurately. This phenomenon has been shown by small scale representation in Figs. 4.7(b) & 4.8(b). Hence, from these simulated curves, it can be said that the proposed chaotic learning based CRTRL algorithm based rotor flux estimation is more accurate than without chaotic learning based CRTRL.



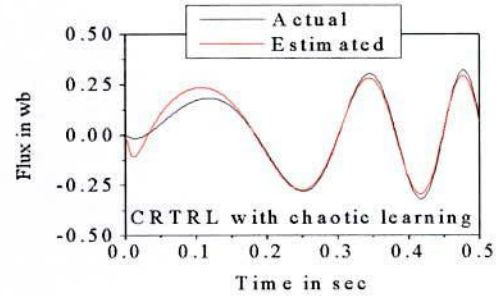
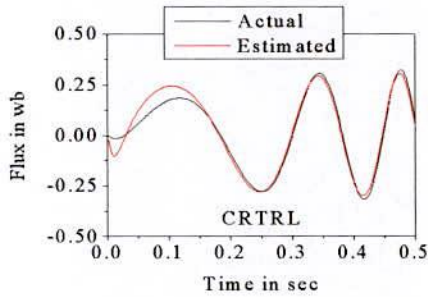
(a)



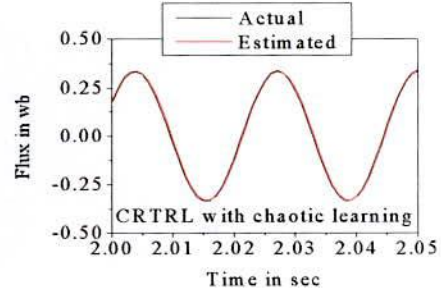
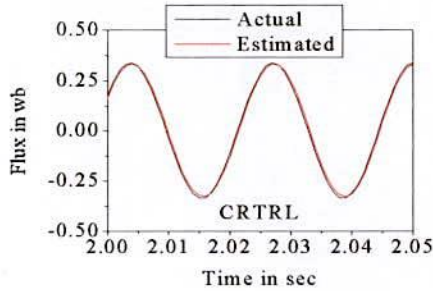


(b)

Figure 4.7  $\alpha$ -axis rotor flux estimation using CRTRL algorithm (a) transient and, (b) steady state.



(a)



(b)

Figure 4.8  $\beta$ -axis rotor flux estimation using CRTRL algorithm (a) transient and, (b) steady state.

#### 4.6 Conclusion

In this chapter chaotic learning based ANNs training has been introduced to estimate the rotor flux components of induction motor drive. Due to the injection of chaos with the learning rates of BP and RTRL, the weight update is accelerated in the local minimum zone. The mean square error of flux estimation improves by 0.00012 and 0.0000175 in the

case of BP and CRTRL algorithms respectively. The rotor flux estimation is also found more accurate at both of transient and steady state conditions due to the use of chaotic learning rate in training of ANNs. As the main condition of high performance induction motor is accurate flux estimation, this proposed work can be used in many industrial applications.

## CHAPTER V

### Proposed Control Methodology and Simulation Study

#### 5.1 Introduction

The efficient and fast control of electric power requires modern technology. It is done by using electronic power converters. The converters transfer energy from a source to a controlled process in a quantized fashion, using semiconductor switches that are turned on and off at fast repetition rates. It is generally preferred to take the power from a DC source and convert it to three-phase AC using DC-to-AC converters. Many technologies are available for this purpose. Space vector modulation (SVM) is one of the technologies. In this research work, a six switch three phase (6S3P) inverter is used with space vector modulation. Simulation studies for proposed high performance induction motor control are presented in this chapter. The gain coefficients of PI controller are optimized using proposed QEA algorithm. The flux is estimated through proposed chaotic learning based CRTRL based ANN. Improvements of the performance of the drive systems are given at the finishing part of the chapter.

#### 5.2 Space Vector Modulation

In voltage controlled drives the reference voltage magnitude and phase angle are generated by the controller. The reference voltage vector  $u^*$  can be resolved into the machine command  $\alpha$ - and  $\beta$ - axes voltages  $v_{\alpha}^*$  and  $v_{\beta}^*$  as:

$$u^* = \sqrt{v_{\alpha}^{*2} + v_{\beta}^{*2}} \quad (5.1)$$

Fig. 5.1 shows the implementation of the SVM principle. The reference vector  $u^*$  is sampled at the clock frequency  $2f_s$ . The sampled reference voltage vector  $u^*(T_s)$  at sampling time  $T_s$  is used to solve the equations to obtain the switching intervals as follows [38]:

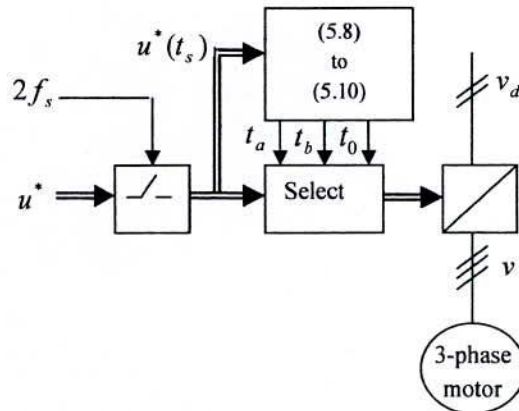


Figure 5.1 Space vector modulation signal flow diagram.

$$\frac{2}{T_s}(t_a u_a + t_b u_b) = u^*(T_s) \quad (5.2)$$

$$t_0 = t_7 = \frac{1}{2}(T_s - t_a - t_b) \quad (5.3)$$

where  $u_a$  and  $u_b$  are the two switching state vectors adjacent in space to the reference vector  $u^*$ , as shown in Fig. 5.2. After solving the above equations the durations  $t_a$ ,  $t_b$  and  $t_0$  of the switching state vectors become:

$$t_a = T_s u^*(T_s) \frac{3}{\pi} \left( \cos \alpha - \frac{1}{\sqrt{3}} \sin \alpha \right) \quad (5.4)$$

$$t_b = T_s u^*(T_s) \frac{2\sqrt{3}}{\pi} \sin \alpha \quad (5.5)$$

$$t_0 = t_7 = \frac{1}{2}(T_s - t_a - t_b) \quad (5.6)$$

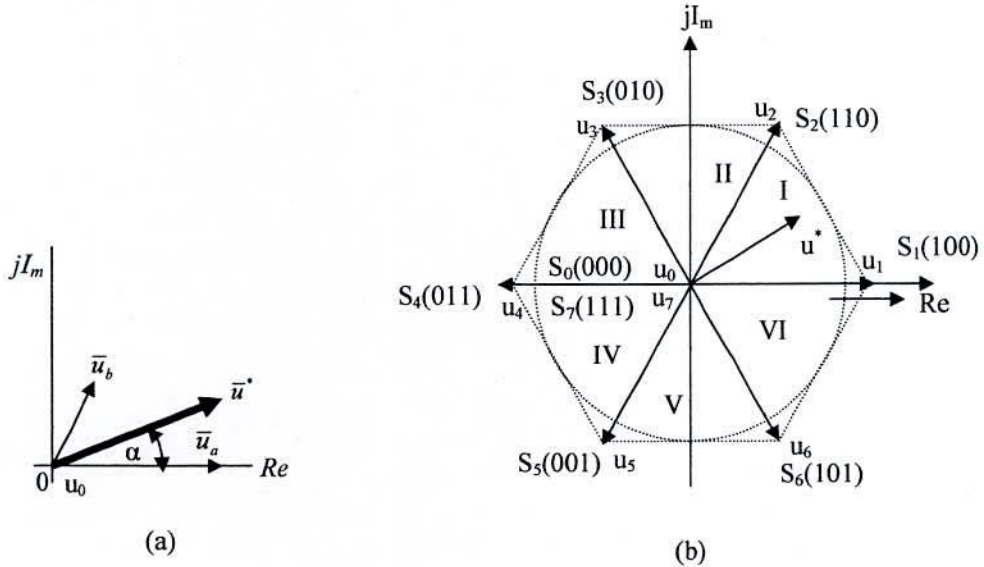


Figure 5.2 (a) Switching-state vectors, shown in the first  $60^\circ$  sector, (b) All voltage vectors in space.

The angle  $\alpha$  in these equations is the phase angle between the reference vector  $u^*$  and  $u_a$ . It is assumed in figure 5.2(a) that the reference vector is located in the first  $60^\circ$  sector of the complex plane. The switching vectors adjacent to the reference vector are  $u_a = u_1$  and  $u_b = u_2$ . When reference vector enters the next sector,  $u_a = u_2$  and  $u_b = u_3$ . Similar sequences are to be maintained for rest of the sectors. The zero vectors are redundant. It can be either formed as  $u_0$  (---), or  $u_7$  (+++). The vector  $u_0$  is preferred when the previous switching-state vector

is  $u_1, u_3$  or  $u_5$ . Similarly  $u_7$  will be chosen when the previous switching vector is  $u_2, u_4$  or  $u_6$ . Hence, the minimum number of commutations is obtained by the switching sequence

$$u_0\langle t_0/2 \rangle \quad u_1\langle t_1/2 \rangle \quad u_2\langle t_2/2 \rangle \quad u_7\langle t_7/2 \rangle \quad (5.7.a)$$

in any first, or generally in all odd subcycles, and

$$u_7\langle t_7/2 \rangle \quad u_2\langle t_2/2 \rangle \quad u_1\langle t_1/2 \rangle \quad u_0\langle t_0/2 \rangle \quad (5.8.b)$$

for the next or all even subcycles. The notation in equations (5.7.a) & (5.7.b) associate to each switching-state vector indicates its on-duration in brackets. Figure 5.2(b) shows all the voltage vectors in space.

### 5.3 Proposed Voltage Vector Based Space Vector Modulation

The dc voltage fed to the inverter is normally constant for voltage source inverters. Voltage magnitude is controlled by modulation in PWM inverters. In this technique there is no scope for adjusting the angular position of the input voltage vector. The forward and backward switching technique for DTC creates chaotic movement of the voltage vector. HPC drives require adjustment of voltage vector magnitude and position for minimum torque pulsation and smooth speed change. Space vector modulation is selected in the present study for better performance of the drive system.

In the proposed control method the torque control aspect of DTC is implemented through the torque control loop that enhances robustness of the control system. On the other hand, fast dynamic speed response is obtained through maintaining the rotor flux constant as in the case of a field orientation control. In DTC both the torque and flux control functions are implemented through inverter switching mechanism. In the proposed methods the control voltages along the rotor flux (d-) axis and perpendicular to its torque (q-) axis are generated and finally SVM principle is used to produce the motor input voltage.

#### 5.3.1 Proposed control scheme

In the proposed scheme shown in Fig. 5.3, the reference torque  $T_e^*$  is generated from torque and speed relation of induction motor. The torque error  $\tau$  is processed through PI controller to generate the q-axis reference current  $i_{qs}^*$ . The d-axis reference current  $i_{ds}^*$  is generated from the machine model directly. The two errors in  $i_{ds}$  and  $i_{qs}$  are also processed through PI controllers to generate reference voltages  $v_{ds}^*$  and  $v_{qs}^*$  respectively. The PI controllers are tuned using QEA to get further fast speed response of IM drive. The rotor flux and torque are estimated using chaotic learning based ANN for accurate rotor position and position sensorless induction motor drive as well.

The reference torque from torque and speed relation of an induction motor is computed by [40-41]:

$$T_e^* = \frac{2J}{p_p} \frac{\dot{\omega}_m^* - \omega_m}{T} + B\omega_m \quad (5.9)$$

Where,

$J$  motor inertia;

$B$  viscous coefficient;

$P_p$  number of pole pairs

$T$  sampling period

The stator command currents are generated as follows:

$$\dot{i}_{ds}^* = \psi_r^* / L_m \quad (5.10)$$

$$\dot{i}_{qs}^* = k_{p1}\tau + k_{i1} \int \tau dt \quad (5.11)$$

Where,  $\tau = T_e^* - T_e$

The symbol  $\hat{\phantom{x}}$  represents the estimated value.

The two command voltages are generated utilizing the two current errors processing through another two PI control loops as:

$$\dot{v}_{qs}^* = k_{p2}(\dot{i}_{qs}^* - \dot{i}_{qs}) + k_{i2} \int (\dot{i}_{qs}^* - \dot{i}_{qs}) dt \quad (5.12)$$

$$\dot{v}_{ds}^* = k_{p3}(\dot{i}_{ds}^* - \dot{i}_{ds}) + k_{i3} \int (\dot{i}_{ds}^* - \dot{i}_{ds}) dt \quad (5.13)$$

Maintaining proper field orientation condition, slip speed is calculated from equation (2.34) as:

$$\omega_{sl} = \frac{1}{\tau_r} \frac{\dot{i}_{qs}^*}{\dot{i}_{ds}^*} \quad (5.14)$$

Here, the estimated slip frequency is optimized by estimating rotor flux accurately using chaotic learning based ANN.

The voltage vector angle  $\theta_v$  combined with the reference rotor flux angle  $\theta_r$  estimated from flux components gives the angle of the input stator voltage needed with respect to the reference stator  $\alpha$ -axis in stationary reference frame ( $\alpha$ - $\beta$ ) of the induction motor model as:

$$\theta_s = \theta_v + \theta_r \quad (5.15)$$

Where,  $\theta_v = \tan^{-1}(\dot{v}_{qs}^* / \dot{v}_{ds}^*)$  and  $\theta_r = \tan^{-1}(\psi_{\beta} / \psi_{\alpha})$ .

The three phase motor currents  $I_a$ ,  $I_b$ , and  $I_c$  are transformed into  $\alpha$ -, and  $\beta$ -axes components through Clarke transformation. Finally, the stationary  $\alpha$ ,  $\beta$ -axis is converted into synchronous  $d$ ,  $q$ -axis to estimate the torque from estimated rotor flux using eq. (2.37).

### 5.3.2 Simulation Model

The two-axes ( $\alpha$ - $\beta$ ) differential equations (2.14 to 2.16) along with torque balance equation (2.5) can be written in discrete form for simulation the model of induction motor as:

$$\begin{aligned} i_{\alpha s}(k+1) = & [R_s / \sigma L_s + R_r(1-\sigma) / \sigma L_s] i_{\alpha s}(k) + [(L_m R_r) / (\sigma L_s L_r^2)] \psi_{\alpha r}(k) \\ & + [\omega_r L_m / \sigma L_s L_r] \psi_{\beta r}(k) + v_{\alpha s}(k) / \sigma L_s \end{aligned} \quad (5.16)$$

$$i_{\beta s}(k+1) = [R_s / \sigma L_s + R_r(1 - \sigma) / \sigma L_s] i_{\beta s}(k) + [\omega_r L_m / \sigma L_s L_r] \psi_{\alpha r}(k) + [(L_m R_r) / (\sigma L_s L_r^2)] \psi_{\beta r}(k) + v_{\alpha s}(k) / \sigma L_s \quad (5.17)$$

$$\psi_{\alpha r}(k+1) = (L_m R_r / L_r) i_{\alpha s}(k) - R_r / L_r \psi_{\alpha r}(k) - \omega_r \psi_{\beta r}(k) \quad (5.18)$$

$$\psi_{\beta r}(k+1) = (L_m R_r / L_r) i_{\beta s}(k) + \omega_r \psi_{\alpha r}(k) - R_r / L_r \psi_{\beta r}(k) \quad (5.19)$$

$$T_d(k+1) = [T_d(k) - T_l - B^* \omega_m(k)] / J \quad (5.20)$$

Where,

$$T_d(k) = 1.5 * P_p [\psi_{\beta r}(k) * [\psi_{\alpha r}(k) - L_m(k) * i_{\alpha s}(k)] / L_r - \psi_{\alpha r}(k) * [\psi_{\beta r}(k) - L_m(k) * i_{\beta s}(k)] / L_r]$$

and  $\sigma = 1.0 - L_m^2 / L_s L_r$ .

The reference control voltages  $v_{ds}^*$  and  $v_{qs}^*$  are generated from (5.12) and (5.13). These voltages and the estimated voltage vector angle  $\theta_v$  are applied to generate the three phase voltages  $v_a, v_b$  and  $v_c$  by SVM principle. The control input to the motor  $v_{\alpha s}^*$  and  $v_{\beta s}^*$  are generated from  $v_a, v_b$  and  $v_c$  by the following transformation:

$$v_{\alpha s}^* = v_a \cos 0^\circ + v_b \cos 120^\circ + v_c \cos 240^\circ \quad (5.21)$$

$$v_{\beta s}^* = v_a \sin 0^\circ + v_b \sin 120^\circ + v_c \sin 240^\circ \quad (5.22)$$

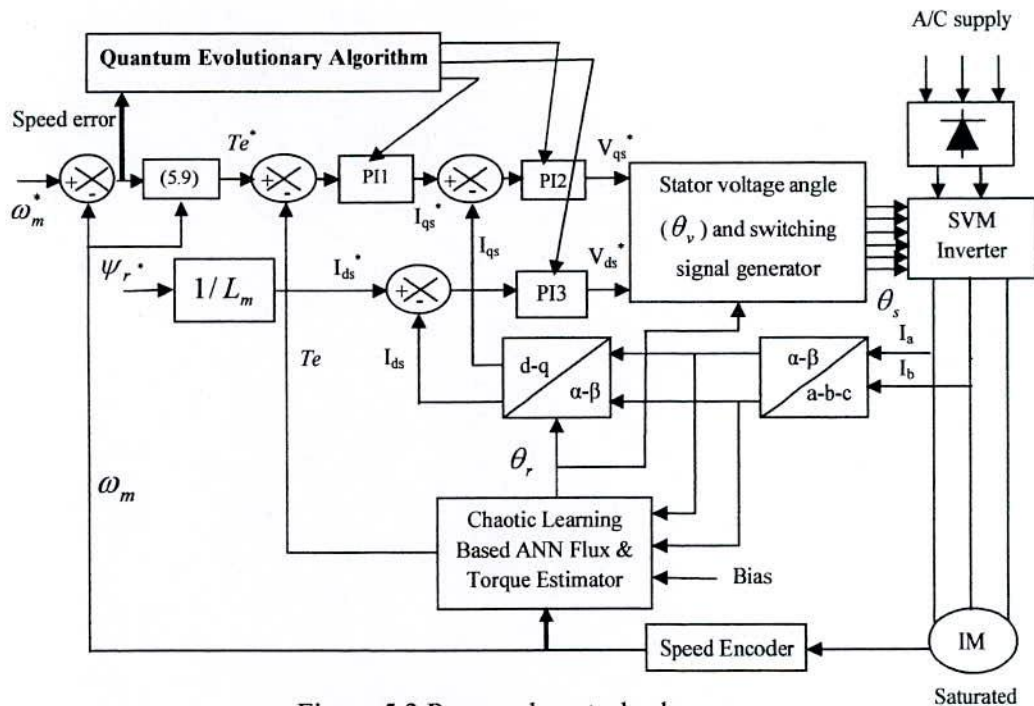


Figure 5.3 Proposed control scheme.

### 5.3.3 The Speed Estimator

A speed estimator is also proposed in this thesis work to make the control system speed sensorless [42-43]. First, the synchronous frequency can be found by noticing the angle of the rotor flux as:

$$\theta_r = \tan^{-1} \left( \frac{\psi_{\beta r}}{\psi_{\alpha r}} \right) \quad (5.23)$$

Taking its derivative:

$$\dot{\theta}_r = \omega_e = \frac{\psi_{\alpha r} \dot{\psi}_{\beta r} - \psi_{\beta r} \dot{\psi}_{\alpha r}}{\psi_{\alpha r}^2 + \psi_{\beta r}^2} \quad (5.24)$$

The rotor speed:

$$\omega_r = \omega_e - \omega_{sl} \quad (5.25)$$

The rotor slip speed  $\omega_{sl}$  can be expressed as follows:

$$\omega_{sl} = R_r \left( \frac{\psi_{\alpha r} i_{\beta s} - \psi_{\beta r} i_{\alpha s}}{\psi_{\alpha r}^2 + \psi_{\beta r}^2} \right) \quad (5.26)$$

Substituting (5.24) and (5.26) in (5.25) the rotor speed can be estimated as:

$$\omega_r = \frac{1}{\psi_r^2} [\psi_{\alpha r} \dot{\psi}_{\beta r} - \psi_{\beta r} \dot{\psi}_{\alpha r} - R_r (\psi_{\alpha r} i_{\beta s} - \psi_{\beta r} i_{\alpha s})] \quad (5.27)$$

Where,  $\psi_r^2 = \psi_{\alpha r}^2 + \psi_{\beta r}^2$

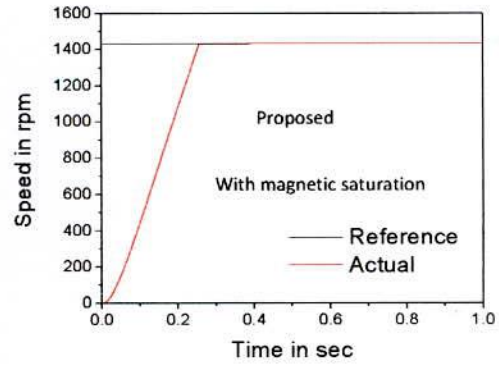
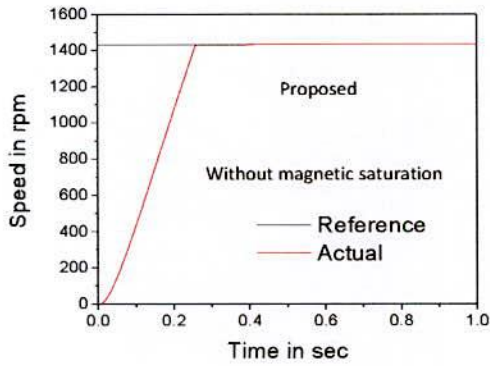
## 5.4 Simulation Study

The proposed control structure is implemented in the environment software C++, and tested with various operating conditions and compared with a recent control system in the dissertation M. A. Rafiq [44], to illustrate the performance of the proposed control scheme. The performance of the proposed control system is justified on the basis of starting time, torque ripple, flux ripple, load disturbance, parameter deviation conditions etc. The flux estimator is trained off-line so that it estimates the flux components accurately. The numerical method for solving the equations is Runge -Kutta method (order 4). Main flux saturation effect has also been considered for more realistic representation in the analysis. The parameters of the induction motor used are given in the appendix.

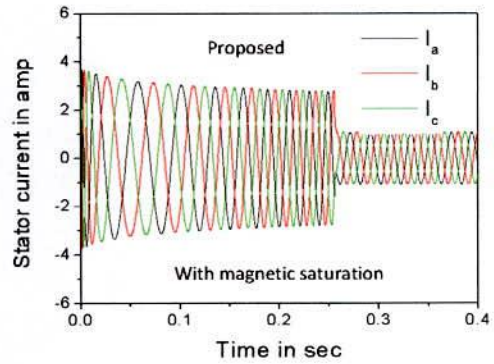
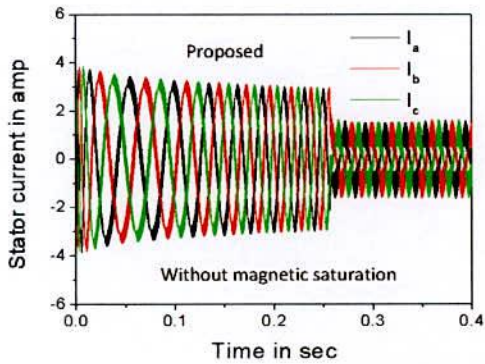
### 5.4.1 Effects of Magnetic Saturation on Induction Motor Drive

Simulation is carried out considering the saturation model of the induction motor using the proposed controller. The significance of considering magnetic saturation are shown in Fig. 5.4. It is observed that the speed responses are almost same, the ripple in stator three phase currents reduced drastically and the fluctuation of developed electromagnetic torque also reduced significantly. It is also observed that the proposed controller draw less current from the supply than that of unsaturated model. Hence, Consideration of magnetic saturation is very much important to achieve actual performance of the drive system as well as high performance controller for induction motor drive.

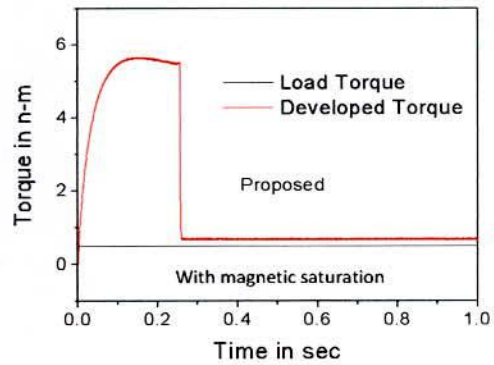
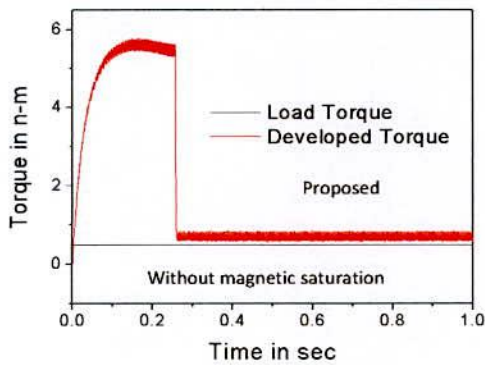




(a)



(b)

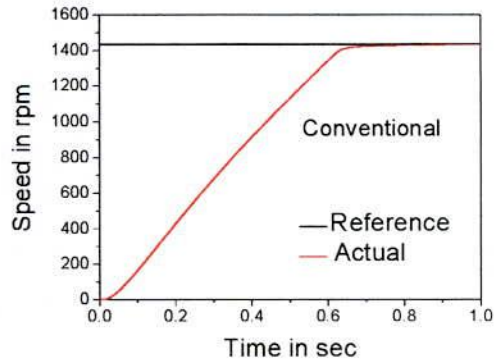
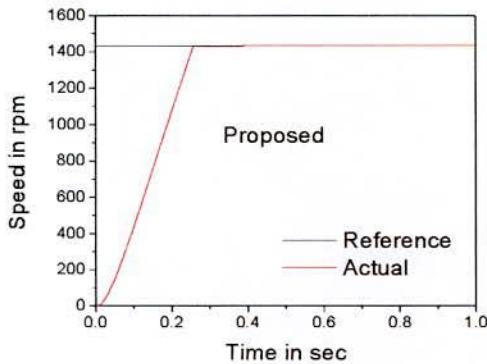


(c)

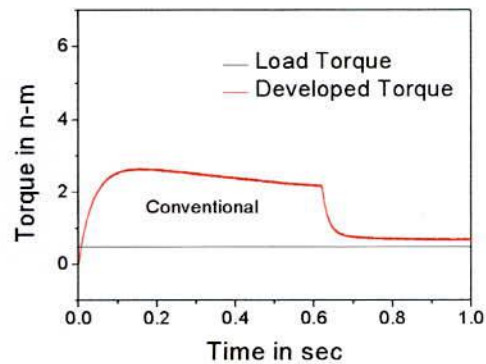
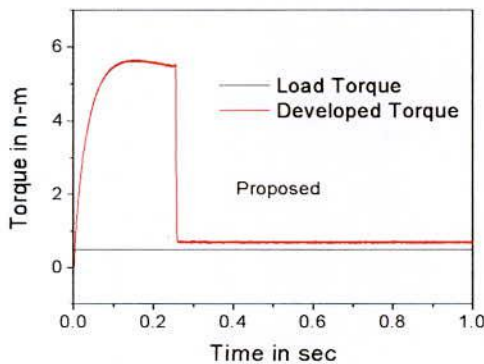
Figure 5.4 Effects of considering magnetic saturation (a) speed response, (b) three phase stator current, and (c) developed electromagnetic torque under transient and steady-state condition.

### 5.4.2 Starting Performance of the Induction Motor Drive

The motor is started with a command speed of 1432 rpm (150 rad/sec) with 0.5 N-m load from standstill condition. At  $t=0.24$  second the motor reaches to the command speed whereas it takes 0.7 second in the conventional controller and shown in Fig. 5.5(a). The motor follows the command speed accurately without steady-state error and oscillations. It can also be seen from Fig. 5.5(b) that, the developed electromagnetic torque is comparatively more and almost ripple free in the proposed control system. The torque ripples reduced by 50% than the conventional control system. In Fig. 5.5(c), it is observed that the rotor flux also follows the reference flux accurately than the conventional control system. So the drive operates perfectly with negligible torque, and flux ripples.

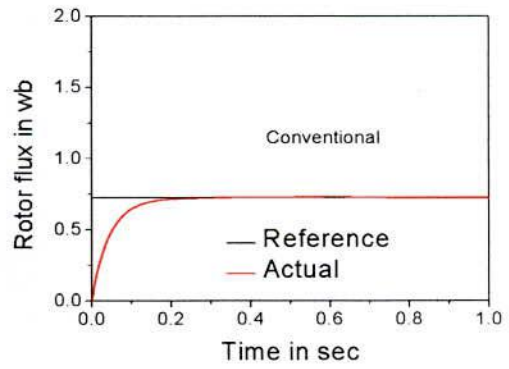
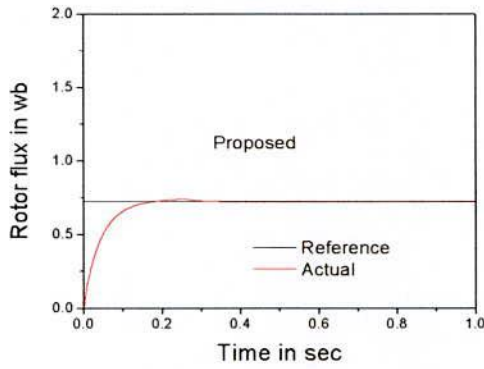


(a)



(b)



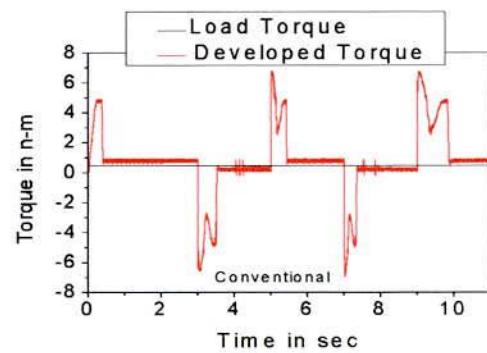
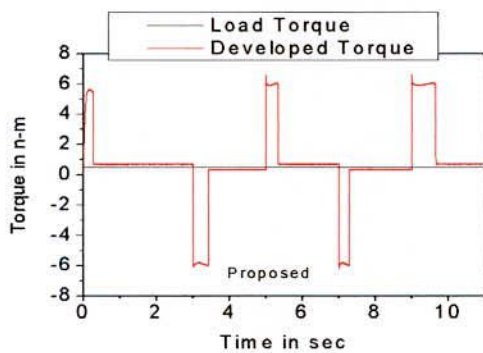
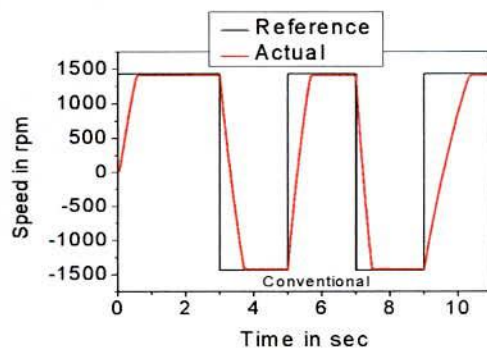
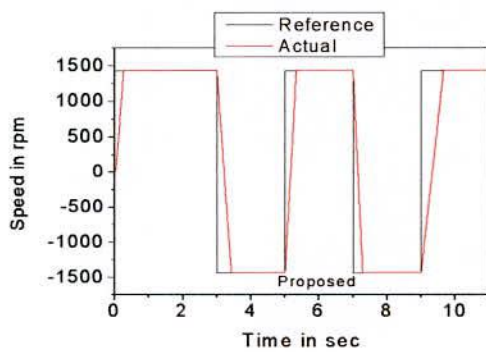


(c)

Figure 5.5 Simulated (a) speed response, (b) developed electromagnetic torque, and (c) rotor flux under transient and steady-state condition.

### 5.4.3 Performance under Different Operating Conditions

The performance of the induction motor drive under different operating conditions is also investigated in order to verify the robustness of the proposed control scheme. The performances of the drive system for different types of change in speed are shown in Figs 5.6(a), 5.6(b), 5.6(c), and 5.6(d). From Fig. 5.6(a) it is observed that the proposed control scheme follows both the forward and reverse direction reference track quickly with negligible torque and flux ripple than the conventional control system. The conventional control system realizes enormous torque pulsation due to the speed reversal condition.



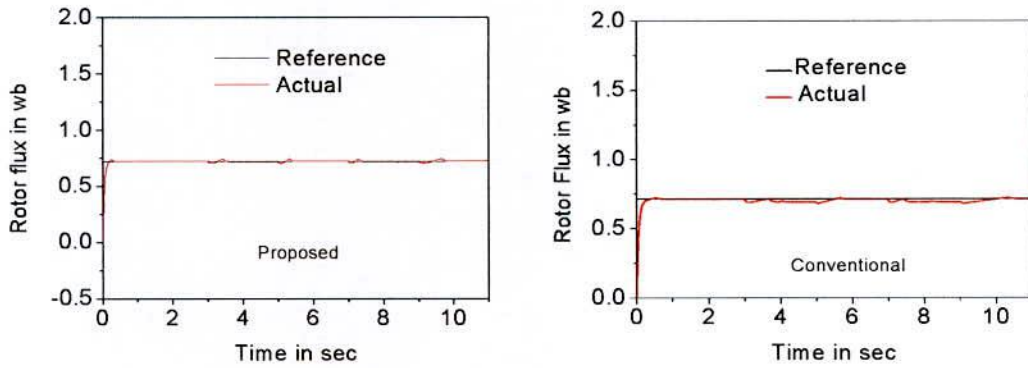


Figure 5.6(a) Performances of the induction motor drive under speed reversal condition at transient and steady state condition.

The proposed control scheme also follows the step change in speed reference track accurately with negligible torque and flux ripple and illustrated in Fig. 5.6(b). In Fig. 5.6(c), the proposed control system maintains the reference ramp change in speed track more accurately than the conventional control system.

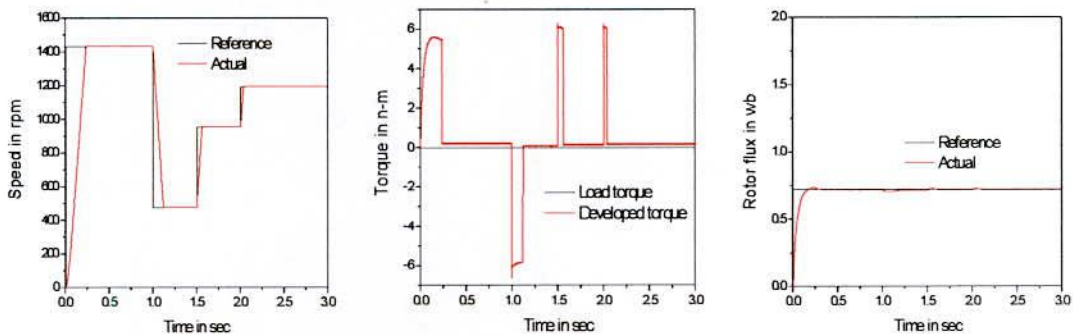
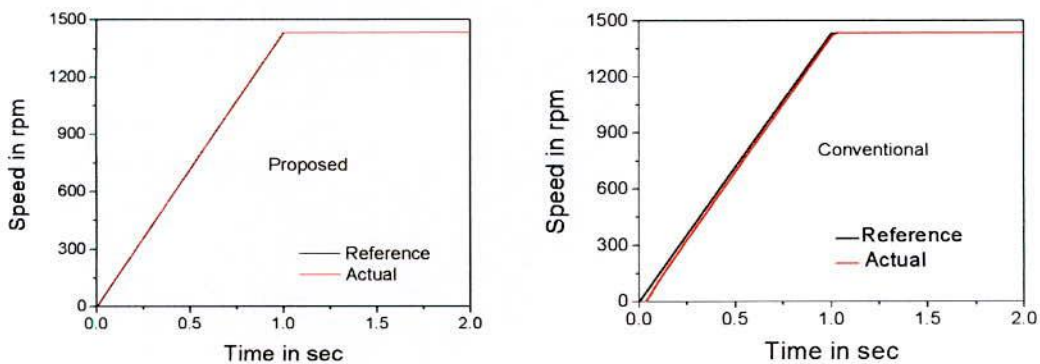


Figure 5.6(b) Performances of the induction motor drive with step change in speed at transient and steady state condition.



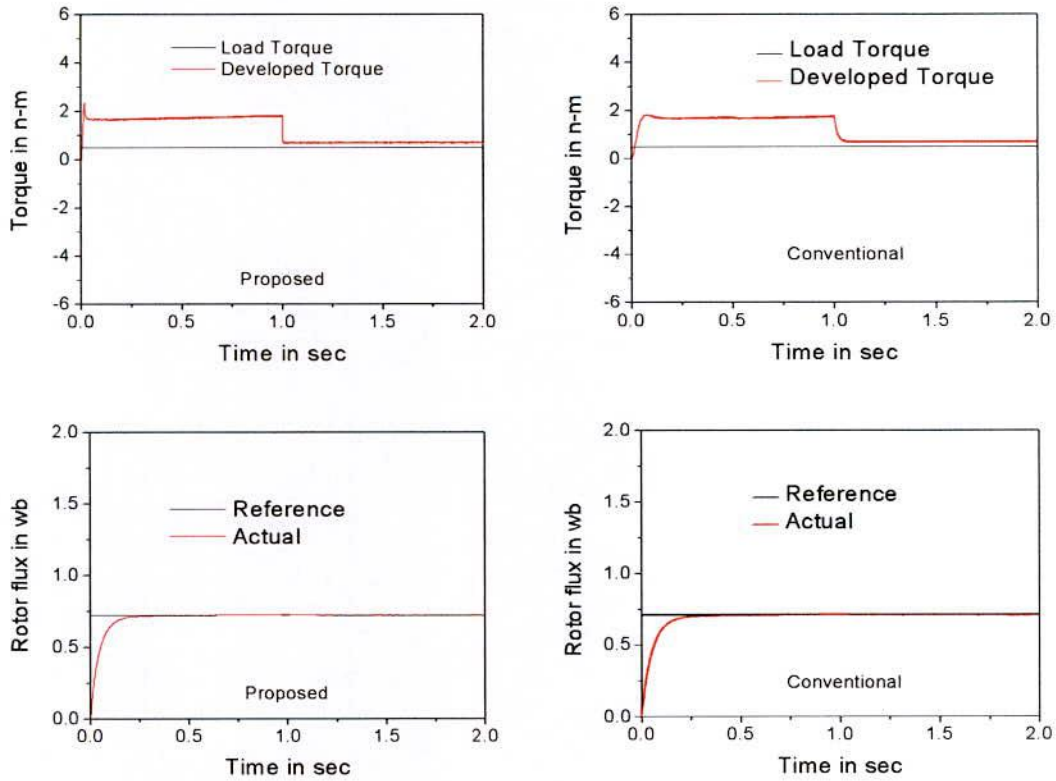
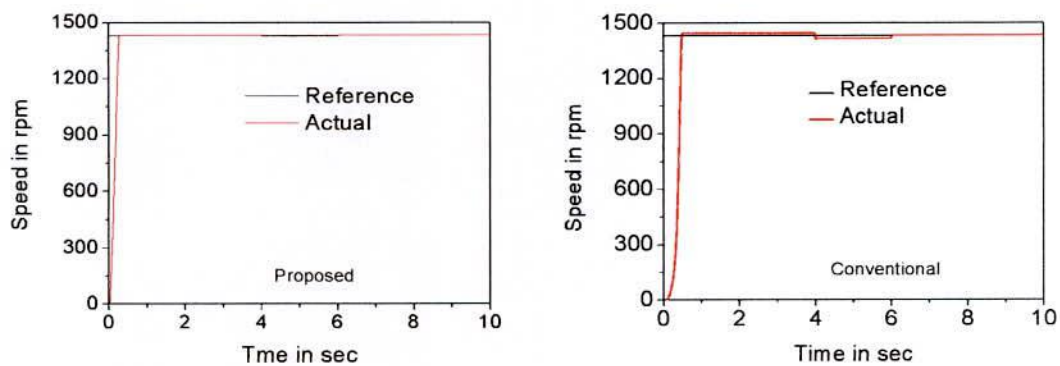
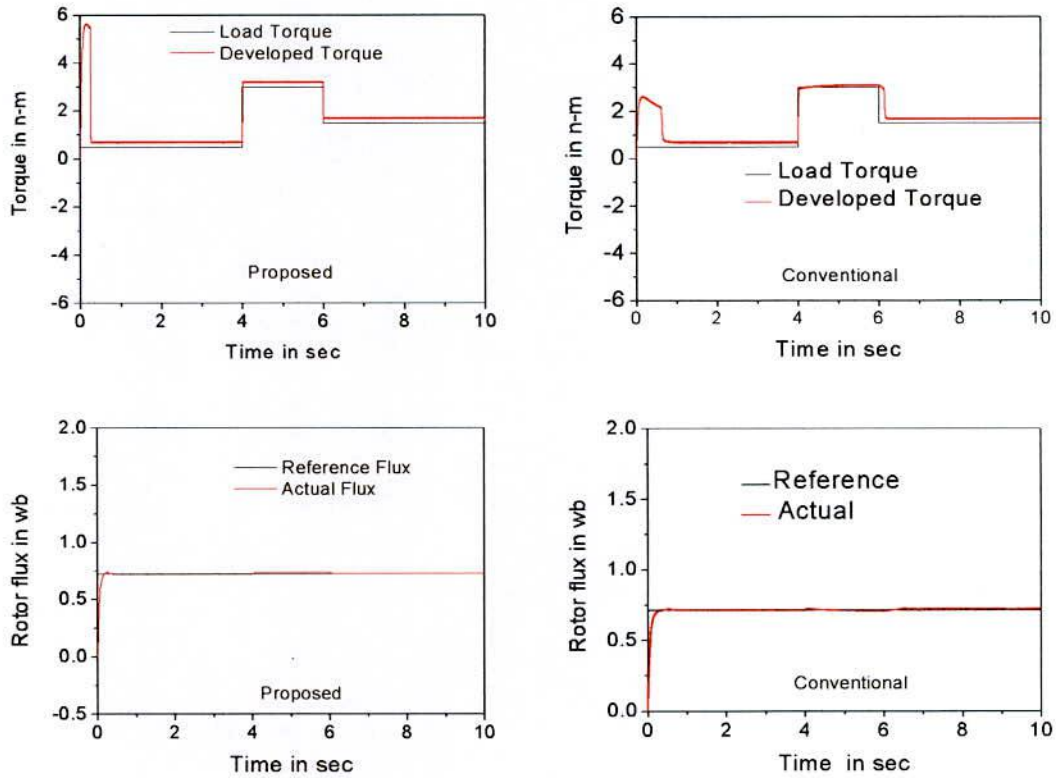


Figure 5.6(c) Performances of the induction motor drive with ramp change in speed at transient and steady state condition.

Effectiveness of the proposed control scheme is also tested by applying and reducing load torque in step and shown in Fig. 5.6(d). The load torque of the motor is suddenly increased from 0.5 N-m to 4.0 N-m at  $t=4.0$  seconds, then decreased to 2.0 N-m at  $t=6.0$  seconds. No fall and oscillation in speed is noticed due to this load torque disturbance whereas the speed falls in the conventional control system due to the sudden application of load. Also the developed electromagnetic torque and the rotor flux are found almost ripple free in the proposed control system.



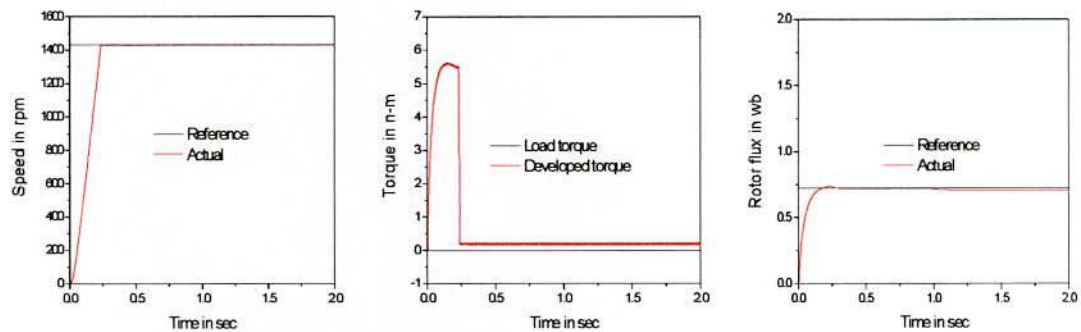


(d)

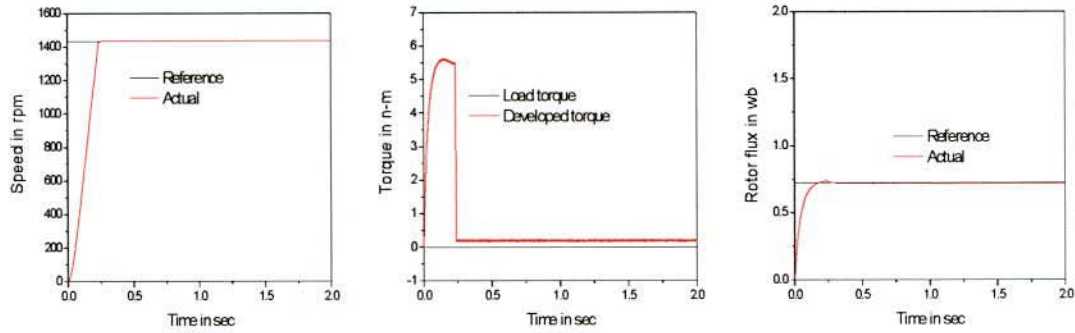
Figure 5.6(d) Performances of the induction motor drive with step change of load at transient and steady state condition.

#### 5.4.4 Performance under Parameter Deviation Conditions

In order to obtain a high performance induction motor drive, its controller should be insensitive with the machine parameter deviation. The insensitivity of the proposed controller due to increase of both stator and rotor resistance of the machine up to 100% from its nominal value at  $t=1.0$  second can be visualized from Fig. 5.7(a) and 5.7(b) respectively.



(a)



(b)

Figure 5.7 Performances of the induction motor drive for change in stator and rotor resistances with (a)  $R_s = 2R_s^*$ , and (b)  $R_r = 2R_r^*$  at  $t=1$  second.

As chaotic learning based ANN is used to estimate the rotor flux directly, the proposed control system is insensitive to rotor resistance deviation condition. But the proposed control system is dependent on the stator resistance deviation condition shown in Fig. 5.7(a).

#### 5.4.5 Robustness against Computational Error

There is some instrumental error always present in physical system. For the robustness test 10% instrumental error is introduced to reference voltage vectors. The performance of the motor speed, developed electromagnetic torque, and the rotor flux are shown in Fig. 5.8. It can be observed that the performances are similar to the motor starting performance. So depending on the performance, it can be concluded that the proposed control scheme is computationally efficient.

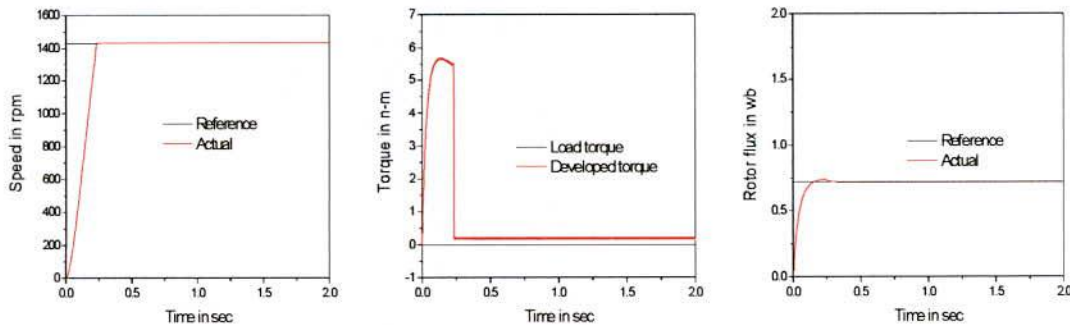
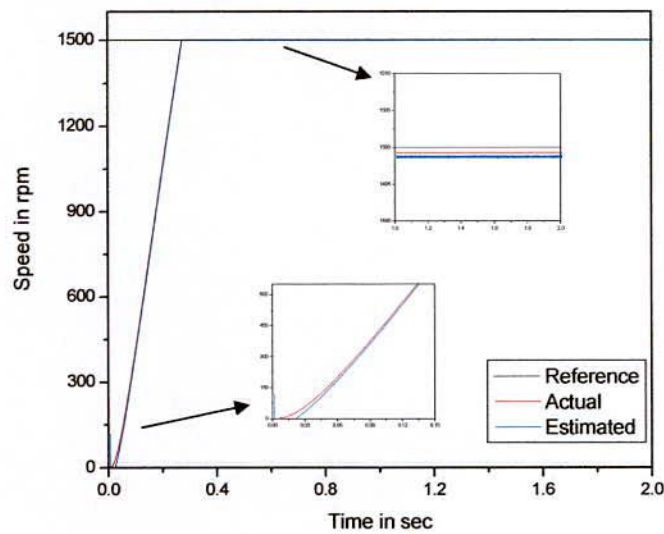


Figure 5.8 Performances of the induction motor drive under computational errors present in the physical system.

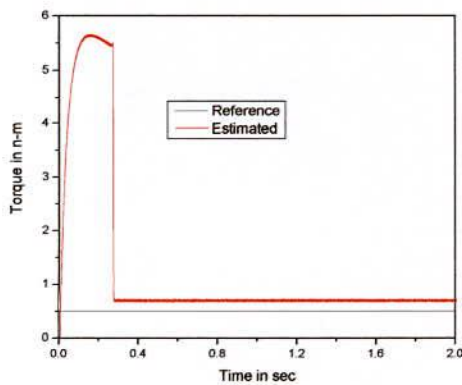
#### 5.4.6 Speed Estimation and Dynamic Behavior

Fig. 5.9 shows the estimated speed, torque and flux responses under transient and steady-state conditions with load torque 0.5 N-m. It is found that the proposed control scheme is capable to estimate the speed accurately at both in transient and steady-state conditions and shown by small scale representation in Fig. 5.9(a). It is confirmed that the proposed speed

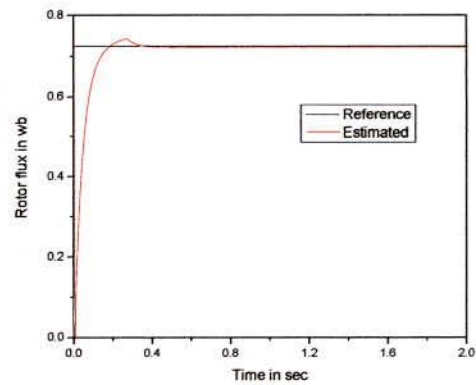
estimator is capable to estimate the speed even at very low speed accurately. From Figs 5.9(b) and 5.9(c), it can be seen that the proposed control system generates negligible torque and flux ripple due to the consideration of main flux saturation effect. Effectiveness of the proposed controller is tested by simulation for different set speed and shown in Fig. 5.10. Negligible overshoot and undershoot is present in the speed estimation and shown by small scale representation in Fig. 5.10. One important matter is noticeable here that if there is no change of speed, there is no overshoot and undershoot in the estimated speed.



(a)



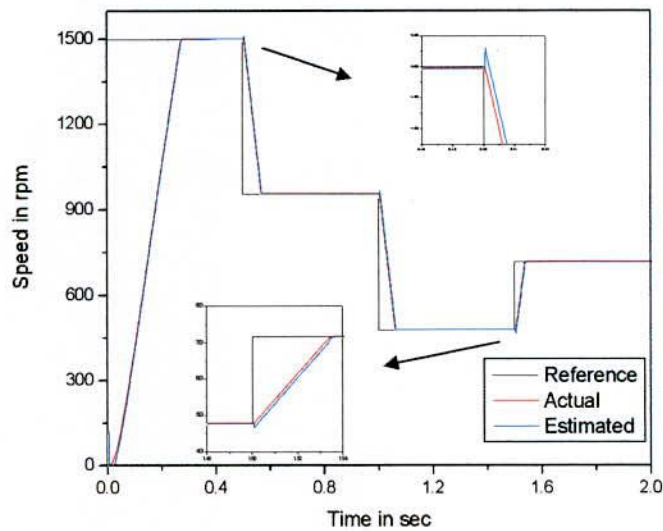
(b)



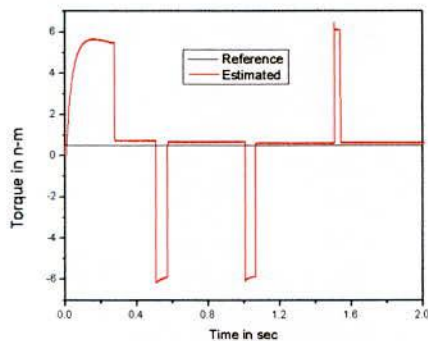
(c)

Figure 5.9 Simulated (a) actual and estimated speed responses (b) estimated electromagnetic torque, and (c) estimated rotor flux under transient and steady-state conditions.

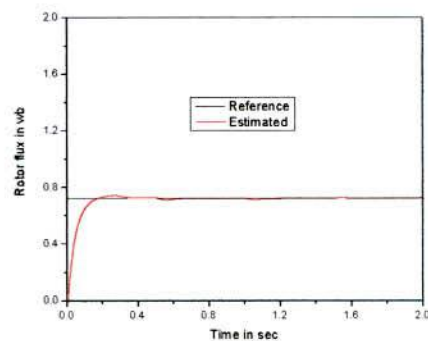




(a)



(b)



(c)

Figure 5.10 Simulated (a) actual and estimated speed responses (b) estimated electromagnetic torque, and (c) estimated rotor flux under transient and steady state conditions.

## 5.5 Conclusion

This chapter present a QEA based high performance control methodology for position sensorless induction motor drive. The proposed DTC-SVM based IM drive with QEA based PI controller and chaotic learning based ANN flux estimator is compared with a conventional control system with classical PI controller and constant learning based CRTRL flux estimator. The results obtained and presented in this work indicate that the proposed control strategy produces fast speed response of the induction motor drive and realizes almost ripple free operation in torque and rotor flux under different situations. The proposed control system provides faster speed response IM drive by 0.46 second and reduced torque ripples by 50% than the conventional control system. The designed control

system is also capable to follow the step change in speed and ramp change in speed accurately whereas the conventional control system cannot track the reference speed accurately. The drive is also robust to load disturbances condition and insensitive to parameter deviation conditions. Chaotic learning based CTRL algorithm turned the control system position sensorless by estimating the rotor flux components accurately at both of transient and steady state conditions. Finally, an endeavor is made to make the proposed control system speed sensorless, more cost effective and practical by estimating the motor speed from very low to rated speed accurately. Due to its simple structure it can be easily implemented on available embedded DSP s, thus it will find many practical applications.

## CHAPTER VI

### Conclusions

#### 6.1 Conclusion

The objective of this Master's thesis was quantum evolutionary algorithm (QEA) based high performance control of induction motor drive in which an effort was made to accommodate the robust and insensitive features of artificial neural network estimator, the fast speed response aspect of DTC processing the speed, torque and flux error and the switching of SVM. The total control law was designed on the consideration of field orientation control with magnetic saturation in IM drive. Step by step development, analysis and study of the proposed methodology have been done in different chapters. The simulation results demonstrate the acceptability of the proposed control methodology for high performance applications.

In this research work, PI controller based voltage vector controlled drive with SVM was used. QEA based PI controller has been used to replace the conventional genetic algorithm based PI controller of induction motor drive system. It was demonstrated that the proposed QEA based PI controller need less time to speed up the motor at transient condition and generate negligible speed fluctuation at rated speed under steady state condition. The gain coefficients of every PI controller in the proposed control system have been tuned by QEA.

The work presented in this dissertation used artificial neural network based flux estimation and suitable control law for high performance control of induction motor drive. For these purposes mathematical models of the three phase induction motor are written in different reference frames under different operating conditions. PI controller based field orientation model and control laws have been designed for the high performance controller. A saturation model of the polyphase induction motor was developed in the study to have more realistic study of the motor drive performance.

The artificial neural network based rotor flux estimator presented in this dissertation has been shown is very accurate and robust to parameter changes. It uses chaotic learning based correlated  $\alpha$  – and  $\beta$  – axes flux estimation and found to work satisfactorily under transient and steady state conditions. Estimated flux components utilized to estimate the position of the rotor flux axis also produce accurate results under steady state and transient conditions. It has been demonstrated that the chaotic learning based backpropagation and CRTRL can estimate the rotor flux more accurately than the same without chaotic learning rate. It can be visualized that the deviation of motor parameters in the machine model has minor significance in the estimated values with a chaotic learning based CRTRL. The chaotic learning based CRTRL estimator has been accepted for flux and angle estimation in designing the high performance drive in this dissertation for its better performance.

The proposed control methodology originates from the speed and torque error processing through controllers instead of instantaneous switching of DTC. The proposed method generates the required voltage components which are used to find out the required voltage magnitude and its position from the inverter. The results of this proposed control system

are compared with the control system having CGA based PI controller and without chaotic learning based CTRL. Very fast speed response, less torque pulsations and capability to work under different operating conditions indicate the efficacy of the proposed control method. It has been observed that the proposed control method is robust against parameter changes and load disturbances. The proposed QEA based PI controller and chaotic learning based ANN flux estimator can be viewed as a part of an effective high performance controller. It is evident from the various simulation results carried out under varying operating conditions. The methodology is inherently designed on the basis of field orientation and accommodates the aspects of SVM based DTC.

Based on the results from the previous chapters and the above discussion it can be concluded that the proposed control scheme provides high performance control for induction motor drives.

## **6.2 Proposal for Further Research**

The dissertation presents a methodology to utilize the artificial intelligence in induction motor control. Different types of flux estimators may be proposed and studied by the researchers working in this area. Future researchers may try with fuzzy-neuro estimators with composite chaotic learning based ANNs. Newly introduced training methods, such as particle swarm optimization or bacterial foraging technique may be tested for training the ANN-Fuzzy estimators. These flux estimators are expected to work effectively under all operating conditions with perturbed parameters. Controller based on ANN-based induction motor model can be used to develop model reference control of the induction motor. On line tuning of the motor model parameters using measurable variables is expected to produce designed results for which the control law is designed.



## References

- 1 C.M. Liaw, Y.S. Kung, and C.M. Wa, "Design and implementation of a high performance field-oriented induction motor drive," *IEEE Trans. Ind. Electron.*, vol. 38, no. 4, pp. 275-282, Aug. 1991.
- 2 G. R. Slemon, "Electric Machines and drives," *Addison-Wesley*, Reading, MA, 1992.
- 3 S. B. Dewan, G. R. Slemon, and A. Straughen, "Power semiconductor drives," *wiley Interscience*, New York, 1984.
- 4 K. B. Nordin, D. W. Novotny, and D. S. Zinger, "The influence of motor parameter deviations in feedforward field orientation drive systems," *IEEE-IAS Trans.*, vol. IA-21, no. 4, pp. 1009-1015, July/August 1985.
- 5 R. D. Lorenz, and D. W. Novotny, "Optimal utilization of induction machines in field oriented drives," *J. Electrical and Electronic Engin.*, Australia, vol. 10, no. 2, pp. 95-100, June 1990.
- 6 G. D. H. Kim, "GA-PSO Based Vector Control of Indirect Three Phase Induction Motor", *Applied Soft Computing*, vol. 7, pp. 601-611, 2006.
- 7 B. Prymak, et al., "Neural Network Based Flux Optimization Using a Model of Losses in Induction Motor Drives", *Mathematics and computers in simulation*, vol. 71, pp. 290-298, 2006.
- 8 S. Ghazzi, K. Jelassi and X. Roboam, "Energy Optimization of Induction Motor Drives", *IEEE conference on Industrial Technology (ICIT)*, pp. 602-610, 2004.
- 9 I. Rechenberg, "Evolution Strategy: Optimization of Technical Systems by Means of Biological Evolution", *Fromman-Holzboog*, 1973.
- 10 L. J. Fogel, A. J. Owens and M. J. Walsh, "Artificial Intelligence through a Simulation of Evolution", In M. Maxfield, A. Callahan And L. J. Fogel, Editors, *Biophysics And Cybernetic Systems. Proc. of the 2<sup>nd</sup> Cybernetic Sciences Symposium*, pp. 131 - 155, Spartan Books, 1965.
- 11 J. H. Holland, "Adaptation in Natural and Artificial Systems: An Introductory Analysis with Applications to Biology, Control, and Artificial Intelligence", *Ann Arbor, MI: University of Michigan Press*.
- 12 J. Kennedy and R. Eberhart, "Particle Swarm Optimization", *IEEE International Conference on Neural Networks (Perth, Australia)*, IEEE Service Center, Piscataway, NJ, pp. IV: 1942-1948, 1995.
- 13 R. Storn and K. Price, "Differential Evolution—A Simple and Efficient Adaptive Scheme for Global Optimization Over Continuous Spaces", *Tech. Rep, International Computer Science Institute, Berkley*, 1995.
- 14 Kuk-Hyun Han and Jong-Hwan Kim, "Quantum-Inspired Evolutionary Algorithm for a Class of Combinatorial Optimization", *IEEE Trans. On Evolutionary Computation*, vol. 6, no. 6, Dec. 2002.

- 15 J. M. Zurada, Introduction to Artificial Neural Systems, *St. Paul, MN: West*, 1992.
- 16 Junwei Ge, Jing Sha, and Yiqiu Fang, "A New Back Propagation Algorithm with Chaotic Learning Rate", *Proceedings of IEEE International Conference on Software Engineering and Service Sciences (ICSESS)*, pp. 404-407, 16-18 July, 2010, Beijing, China.
- 17 M. Islam, M. R. Rana, S. U. Ahmed, A. N. M. Enamul Kabir, and M. Shahjahan, "Training Neural Network with Chaotic Learning Rate", *Proceedings of International Conference on Emerging Trends in Electrical and Computer Technology (ICETECT)*, pp. 781-785, 23-24 March 2011, Tamil Nadu, India.
- 18 B. K. Bose, "Expert system, fuzzy logic and neural network application in power electronics and motion control," *Proc. IEEE*, vol. 82, no. 8, pp. 1303-1323, Aug. 1994.
- 19 L. E. B. Da Silva, B. K. Bose, and J.O.P. Pinto, "Recurrent-neural-network-based implementation of a programmable cascaded low-pass filter used in stator flux synthesis of vector-controlled induction motor drive", *IEEE Transactions on Industrial Electronics*, vol. 46, issue 3, pp. 662-665, June 1999.
- 20 Md. Abdur Rafiq, Naruttam Kumar Roy, and B.C. Ghosh, "An Improved Induction Motor Rotor Flux Estimator Based on Correlated Real Time Recurrent Learning Algorithm", *Proceedings of the International Conference on Power System Analysis*, Visakhapatnam, AP, India, pp. 866-873, 2008.
- 21 Cui Wei, K. T. Chau, Wang Zheng, and J. Z. Jiang, "Application of Chaotic Modulation to AC Motors for Harmonic Suppression", *Proc. of IEEE International Conference on Industrial Technology (ICIT)*, pp. 2343-2347, 15-17 Dec. 2006, Mumbai, India.
- 22 D. C. Huynh, M. W. Dunnigan, and S. J. Finney, "Vector Controlled Induction Motor Drives Based on Chaotic SVPWM", *Transactions of China Electrotechnical Society*, 2009-11.
- 23 D. C. Huynh, M. W. Dunnigan, and S. J. Finney, "Energy efficient control of an induction machine using a chaos particle swarm optimization algorithm", *Proc. of IEEE International Conference on Power and Energy (PECon)*, pp. 450-455, Nov. 29 2010-Dec. 1 2010, Kuala Lumpur, Malaysia.
- 24 Bambang Purwahyudi, Soebagio, and M. Ashari, "RNN Based Rotor Flux and Speed Estimation of Induction Motor", *International Journal of Power Electronics and Drive System (IJPEDS)*, vol.1, no.1, pp. 58-64, September 2011.
- 25 A Derdiyok, "Speed sensorless control of induction motor using a continuous control approach of sliding-mode and flux observer," *IEEE Trans. Ind. Electron*, vol. 52, no. 4, 2000, pp. 1170-1176.
- 26 C Lascu, I Boldea and F Blaabjerg, "Direct torque control of sensorless induction motor drives: A sliding mode approach," *IEEE Trans. Ind. Applicat.*, vol. 40, no. 2, 2004, pp. 582-590.

- 27 C Lascu, I Boldea and F Blaabjerg, "Very-low-speed variable-structure control of sensorless induction machine drives without signal injection," *IEEE Trans. Ind. Applicat.*, vol. 41, no. 2, 2005, pp. 591-598.
- 28 P Vaclavek and P Blaha, "Lyapunov-function-based flux and speed observer for AC induction motor sensorless control and parameter estimation," *IEEE Trans. Ind. Electron.*, vol. 53, no. 1, 2006, pp. 138-145.
- 29 MJ Duran, JL Duran, F Perez and J Fernandez, "Induction-motor sensorless vector control with on-line parameter estimation and over-current protection," *IEEE Trans. Ind. Electron.*, vol. 53, no. 1, 2006, pp. 154-161.
- 30 Jansen, P. L., R. D. Lorenz, and D. W. Novotny, 1993, "Observer-based field orientation: Analysis and comparison of alternative methods", *IEEE Industry Application Society, Annual Meeting Conf. Rec. October, Part 1*, pp. 536-543.
- 31 Van Wyk, J. D., H-chi. Skudelny, and A. Müller Hellman, 1986, "power electronics, control of the electromechanical energy conversion process and some applications", *proc. Inst. Elec. Eng.*, November, vol. 133, part B, pp. 369-399,. Also in B. K. Bose (ed.), 1992, "Modern Power Electronics", *IEEE Press*, New York, NY, pp. 43-73.
- 32 S. N. Bhadra, 1982, "A direct method of predict instantaneous saturation curve from rms saturation curve", *IEEE Transactions on Magnetics*, November, Vol. Mag-18, No.6, pp. 1867-1869.
- 33 Seung Ki Sul, and Min Ho Park, 1988, "A novel technique for optimal efficiency control of a current-source inverter-fed induction motor", *IEEE Transactions on Power Electronics*, April, Vol.3, No.2, pp. 192-198.
- 34 Watanabe Keigo, Hashem M.M.A. 2004, "New Algorithms and their Applications to Evolutionary Robots", Series: Studies in Fuzziness and Soft Computing, Vol. 147, *Springer-Verlag*, Berlin/New York, ISBN: 3-540-20901-8.
- 35 Md. Habibullah, Md. Amjad Hossain, Md. Abdur Rafiq, and B. C. Ghosh, "Quantum Evolutionary Algorithm based Fast Speed Controlled Induction Motor Drive with CRTRL Flux Estimator", *proc. of IEEE International Conference on Electrical and Computer Engineering (ICECE-2010)*, pp. 478-481, 18-20 Dec. 2010, Dhaka, Bangladesh.
- 36 Simon Haykin, 2001, "Neural networks a comprehensive foundation", 2<sup>nd</sup> edition, *Pearson education, Inc.*
- 37 Md. Habibullah, Md. Abdur Rafiq, Md. Shahjahan, and B. C. Ghosh, "Chaotic Learning Based ANN for Improved Rotor Flux Estimation of Induction Motor Drive", accepted by *International Conference on Informatics, Electronics & Vision (ICIEV12)*, May 18-19, 2012, Dhaka, Bangladesh.
- 38 Md. Abdur Rafiq, Naruttam Kumar Roy, and B. C. Ghosh, "Three algorithms for learning artificial neural network: A comparison for induction motor flux estimation," *Proc. of 12<sup>th</sup> International conf. on computers and information technology*, pp. 355-360, Dec. 21-23, 2009, Dhaka, Bangladesh.

- 39 Bimal K. Bose, 1996, "Power Electronics and Variable Frequency Drives, Technology and Applications", *IEEE press*, Piscataway.
- 40 Jae Ho Chang, and Byung Kook Kim, "Minimum-Time Minimum Loss Speed Control of Induction Motors Under Field-Oriented Control," *IEEE Trans. on Ind. Electron.*, vol. 44, no.6, Dec. 1997, pp. 809-815.
- 41 Md. Habibullah, Md. Jahirul Islam, Md. Abdur Rafiq, Kalyan Kumar Halder, and B. C. Ghosh, "A New DTC-SVM Based Control of Field Oriented Position Sensorless Induction Motor Drive with Reduced Torque and Flux Ripple," *International Journal of Computer and Electrical Engineering (IJCEE)*, Vol. 3, No. 3, pp. 327-334, June 2011.
- 42 Md. Habibullah, Md. Abdur Rafiq, and B. C. Ghosh, "A New QEA Based High Performance Sensorless Control of IM Drive", *Proc. of Int. Conf. on Advances in Electrical & Electronics 2011*, pp. 55-59, 20-21 Dec., 2011.
- 43 Md. Habibullah, Kalyan Kumar Halder, Md. Abdur Rafiq, and B. C. Ghosh, "High Performance Sensorless Control of Induction Motor Drive with Space Vector Modulation", *Proc. of Int. Conf. on Advances in Electrical Engineering 2011*, pp. 154-159, 19-20 Dec., 2011.
- 44 Md. Abdur Rafiq, "Artificial Neural Network Based High Performance Control of Induction Motor Drive", Ph.D. Thesis, Department of Electrical and Electronic Engineering, KUET, Khulna, September 2009.



## APPENDIX

**Table App. 1 Induction Motor Parameters and Nameplate Data / Rating**

**Nameplate data:** 3-phase, 50Hz, 415V, 1.8A, 0.75KW, 0.8 p.f., 4- pole, Y-connected

**Parameters:**

Sl. No	Nominal Parameters (referred to stator)	Values in SI units
1	Stator resistance, $R_s$	13.25 $\Omega$
2	Rotor resistance, $R_r$	16.818 $\Omega$
3	Mutual inductance, $L_m$	0.7114H
4	Stator self inductance, $L_s$	0.7359H
5	Rotor self inductance, $L_r$	0.7359H
6	Moment of inertia, $J$	0.0075kg-m <sup>2</sup>
7	Damping coefficient, $B$	0.00107Nm-sec/rad

## List of Publications

### International Journals:

1. **Md. Habibullah**, and B. C. Ghosh, "Quantum-Inspired Evolutionary Algorithm Based PI Controller Tuning for High Performance Induction Motor Drive with Improved Flux Estimator", *International Journal of Computing and Applications (IJCA)*, Vol. 6, No. 1, pp. 55-60, January-June 2011, ISSN: 0973-5704.
2. **Md. Habibullah**, Md. Jahirul Islam, Md. Abdur Rafiq, Kalyan Kumar Halder, and B. C. Ghosh, "A New DTC-SVM Based Control of Field Oriented Position Sensorless Induction Motor Drive with Reduced Torque and Flux Ripple", *International Journal of Computer and Electrical Engineering (IJCEE)*, Vol. 3, No. 3, pp. 327-334, June 2011, ISSN: 1793-8163.

### International Conference Papers:

3. **Md. Habibullah**, Md. Amjad Hossain, Md. Abdur Rafiq, and B. C. Ghosh, "Quantum Evolutionary Algorithm based Fast Speed Controlled Induction Motor Drive with CRTRL Flux Estimator", *proc. of IEEE International Conference on Electrical and Computer Engineering (ICECE-2010)*, pp. 478-481, 18-20 Dec. 2010, Dhaka, Bangladesh.
4. **Md. Habibullah**, Md. Abdur Rafiq, and B. C. Ghosh, "A New QEA Based High Performance Sensorless Control of IM Drive", *Proc. of Int. Conf. on Advances in Electrical & Electronics 2011*, pp. 55-59, 20-21 Dec., 2011, New Delhi, India.
5. **Md. Habibullah**, Kalyan Kumar Halder, Md. Abdur Rafiq, and B. C. Ghosh, "High Performance Sensorless Control of Induction Motor Drive with Space Vector Modulation", *Proc. of Int. Conf. on Advances in Electrical Engineering 2011*, pp. 154-159, 19-20 Dec., 2011, Dhaka, Bangladesh.
6. **Md. Habibullah**, Md. Abdur Rafiq, Md. Shahjahan, and B. C. Ghosh, "Chaotic Learning Based ANN for Improved Rotor Flux Estimation of Induction Motor Drive", accepted by *International Conference on Informatics, Electronics & Vision (ICIEV12)*, May 18-19, 2012, Dhaka, Bangladesh.